Impacts of condensable particulate matter on atmospheric organic aerosols and fine particulate matter ($PM_{2.5}$) in China

Mengying Li[1], Shaocai Yu[1+], Xue Chen[1], Zhen Li[1], Yibo Zhang[1], Zhe Song[1], Weiping Liu[1], Pengfei Li[2+], Xiaoye Zhang[1,3], Meigen Zhang[4,5,6], Yele Sun[4,5], Zirui Liu[4,5], Caiping Sun[7], Jingkun Jiang[8,9], Shuxiao Wang[8], Benjamin N. Murphy [10], Kiran Alapaty[10], Rohit Mathur[10], Daniel Rosenfeld[11], and John H. Seinfeld[12]

[1]Research Center for Air Pollution and Health; Key Laboratory of Environmental Remediation and Ecological Health, Ministry of Education, College of Environment and Resource Sciences, Zhejiang University, Hangzhou, Zhejiang 310058, P.R. China

[2]College of Science and Technology, Hebei Agricultural University, Baoding, Hebei 071000, P.R. China

[3]Chinese Academy of Meteorological Sciences, China Meteorological Administration, Beijing 100081, China.

[4]State Key Laboratory of Atmospheric Boundary Layer Physics and Atmospheric Chemistry (LAPC), Institute of Atmospheric Physics (IAP), Chinese Academy of Sciences (CAS), Beijing 100029, China

[5]University of Chinese Academy of Sciences, Beijing 100049, China

[6]Center for Excellence in Urban Atmospheric Environment, Institute of Urban Environment, Chinese Academy of Sciences, Xiamen, China

[7]Chinese Research Academy of Environmental Sciences, Beijing 100012, China

[8]State Key Joint Laboratory of Environment Simulation and Pollution Control, School of Environment, Tsinghua University, Beijing 100084, China

[9]State Environmental Protection Key Laboratory of Sources and Control of Air Pollution Complex, Beijing 100084, China

[10]Center for Environmental Measurement and Modeling, U.S. Environmental Protection Agency, Research Triangle Park, NC 27711, USA

[11]Institute of Earth Sciences, The Hebrew University of Jerusalem, Jerusalem, Israel

[12]Division of Chemistry and Chemical Engineering, California Institute of Technology, Pasadena, CA 91125, USA.

[+]*Correspondence to*: Shaocai Yu (shaocaiyu@zju.edu.cn); Pengfei Li (lpf_zju@163.com)

To be submitted to

Atmospheric Chemistry and Physics

Abstract

Condensable particulate matter (CPM) emitted from stationary combustion and mobile sources exhibits high emissions and a large proportion of organic components. However, CPM is not generally measured when conducting emission surveys of PM in most countries, including China. Consequently, previous emission inventories have not included emission rates for CPM. Here we construct an emission inventory of CPM in China with a focus on organic aerosols (OA) based on collected CPM emission information. Results show that OA emissions are enhanced twofold after the inclusion of CPM in a new China inventory for the years 2014 and 2017. Considering organic CPM emissions and model representations of secondary OA (SOA) formation from CPM, here a series of sensitivity cases have been simulated using the three-dimensional Community Multiscale Air Quality (CMAQ) model to estimate the contributions of CPM emissions to atmospheric OA and fine PM ($PM_{2.5}$) concentrations in China. Compared with observations during a haze episode from October 14 to November 14, 2014, at a Beijing site, estimates of temporal average primary OA (POA) and SOA concentrations are greatly improved after including the CPM effects. These scenarios demonstrated the significant contributions of CPM emissions from stationary combustion and mobile sources to POA (51 ~ 85%), SOA (42 ~ 58%), and total OA concentrations (45 ~ 75%). Furthermore, contributions of CPM emissions to total OA concentrations were demonstrated over the major 2+26 cities of Beijing-Tianjin-Hebei region (BTH2+26 cities) in December 2018, with average contributions up to 49%, 53%, 54%, and 50% for Handan, Shijiazhuang, Xingtai, and Dezhou, respectively. Correspondingly, the inclusion of CPM emissions also narrowed the gap between simulated and observed $PM_{2.5}$ concentrations over the BTH2+26 cities. These results improve the simulation performance of atmospheric OA and $PM_{2.5}$, and may provide important implications for the sources of OA.

1 Introduction

Atmospheric fine particulate matter ($PM_{2.5}$, particulate matter with aerodynamic diameter not exceeding 2.5 μm) is a serious and recurring air quality problem. Although the annual average concentration of $PM_{2.5}$ in China has declined in recent years, it still exceeds standards promulgated by the World Health Organization (WHO) Air Quality Guidelines (Lin et al., 2018). Heavy haze episodes occur frequently in winter, especially for the eastern regions in China (Li et al., 2015; Chen et al., 2019; Li et al., 2017a). Despite large reductions in primary emissions during the COVID-19 lockdown, several periods of heavy haze continued to occur in eastern China (Huang et al., 2021; Wang et al., 2020c, 2021). Organic aerosols (OA) contribute a large fraction to $PM_{2.5}$ worldwide, ranging from 20% to 90% (Carlton et al., 2009; Kanakidou et al., 2005) with a negative radiative forcing and adverse impacts on air quality and human health (Gehring et al., 2013; Pope et al., 2002). POA comes from a variety of sources, including fossil fuels and biomass burning. SOA is generated through photochemical oxidation of volatile organic compounds (VOCs) followed by gas-particle partitioning of low-volatility organic compounds into the aerosol phase (Fuzzi et al., 2006; Kroll and Seinfeld, 2008) Currently, the significant contributions of OA to $PM_{2.5}$ and SOA to OA have been demonstrated in many observational results (He et al., 2020; Veld et al., 2021; Zhang et al., 2017). For example, Huang et al. (2014) explored the role of OA in $PM_{2.5}$ during a severe haze episode in Beijing, Shanghai, Xi'an and Guangzhou, showing the substantial contribution of OA to $PM_{2.5}$ (30~50%) and SOA accounted for 30~77% of OA. Sun et al. (2015) showed that OA constituted up to 65% of submicron aerosols during winter in Beijing, with 38% being SOA.

With respect to chemical schemes of SOA formations, a two-product model (Odum et al., 1996) was first proposed based on absorptive partitioning theory (Pankow, 1994) and chamber data. To address the underestimation of the early two-product model, the volatility basis set (VBS) framework was developed (Donahue et al., 2006). In this VBS scheme, semi-volatile and intermediate volatility precursors (S/IVOCs) were classified by their volatilities based on the absorptive partitioning theory (Robinson et al., 2007). A large portion of SVOCs are emitted as POA and then evaporate at ambient conditions due to gas-particle partitioning, while the IVOCs species exist in the form of organic vapor under many atmospheric conditions in the absence of photochemical reactions (Shrivastava et al., 2011). Currently, the VBS mechanism has been incorporated into many global and regional scale models (Lane et al., 2008; Murphy and Pandis, 2009; Shrivastava et al., 2008; Han et al., 2016). The two-dimensional (2-D) VBS scheme was put forward to improve the accuracy of fragmentation processes and OA oxidations (Donahue et al.,

2011; Zhao et al., 2016). Despite advances in SOA formation mechanisms, a gap exists between observed and modeled results due to uncertainties in parameterization of SOA yields, lack of localized parameters and incomplete information on emission rates and properties of SOA precursors. Recent studies have begun to focus on important effects of emissions, including traditional precursors (VOCs) and S/IVOCs. For example, Zhao et al. (2017) found that IVOCs of 1.5–30 times POA emissions contributed largely to OA concentrations over the BTH region. Wu et al. (2019) constructed an inventory of S/IVOCs for the Pearl River Delta (PRD) region in China and conducted a simulation using the WRF-Chem model leading to an increase of 161% in SOA predictions. Emissions of S/IVOCs from mobile sources and IVOCs from volatile chemical products were also parameterized in models to represent SOA formation (Jathar et al., 2017; Lu et al., 2020; Pennington et al., 2021). Although the significant role of potential emission sources in OA formation has been demonstrated, underestimation of SOA by current air quality models has not been completely resolved. Stationary combustion sources are one of the major emission sources of $PM_{2.5}$, including power plants and factories. Sampling temperatures and dilution rates are key factors for accurate measurements of organic matter (Morino et al., 2018). The total primary PM emitted from stationary sources is composed of filterable PM (FPM) and condensable PM (CPM). FPM exists in liquid or solid phases, while CPM is in gas phase in flue (Corio and Sherwell, 2000; Feng et al., 2018). CPM is defined by the U.S. Environmental Protection Agency (EPA, 2017) as particles which are gaseous at flue gas temperature but condense or react in the ambient air to form solid or liquid PM through dilution and cooling immediately after discharge. With ultralow emission standards implemented by coal-fired power plants (<10 mg Nm^{-3}) since 2014, FPM emissions have been substantially reduced (even below 5 mg Nm^{-3}) (Tang et al., 2019), making the remaining emissions of CPM an important issue. The Ministry of Science and Technology of China issued a national key research and development project on the causes and controls of air pollution in 2016, which mentioned key technologies for controlling CPM emissions (http://www.acca21.org.cn/zdy_cms/siteResources/DisasterReduction/resources/otherfiles/20160425/f15345793.pdf). The current measurement studies about emission characteristics and chemical composition of CPM exhibited non-negligible emissions. For example, Yang et al. (2014, 2018a, 2018b) conducted investigations for different types of industrial boilers and power plants, and concluded that CPM constituted 25.7~96.5% of $PM_{2.5}$. For an ultralow-emission coal-fired power plant, Li et al. (2017b) reported that the emission concentrations of CPM accounted for 83% of the $PM_{2.5}$. Wang et al. (2018) calculated the average emission factors of CPM from two stacks in a waste incineration power plant to be 0.201 and 0.178 g kg^{-1}, which were 22.0 and 31.2 times higher than the corresponding those of FPM,

respectively. Wu et al. (2020) found that FPM emissions from four typical coal-fired power plants met Chinese ultra-low emission standards, while CPM showed high levels (even above 10 mg Nm^{-3}). CPM includes organic and inorganic components, known as organic CPM and inorganic CPM, respectively. The contributions of organic fractions varied from 13.6% to 80.5%, depending on different fuel types, test methods and operating conditions (Lu et al., 2019; Song et al., 2020; Yang et al., 2021, 2018b). Many studies confirmed that CPM contained more than 50% organic components (Li et al., 2017c, 2017d; Song et al., 2020; Wu et al., 2020), revealing that organic matter comprising a large proportion in CPM needed to be taken into account. These above studies provided valuable basic information of CPM emission characteristics for data references in this study, as summarized in Table S3. It is likely that the inorganic fractions of CPM make a contribution to the water-soluble ions in $PM_{2.5}$, and organic components contribute to the organic matter in $PM_{2.5}$. In addition, large amounts of low volatile organic compounds in CPM can be important precursors for SOA formation.

Current measurement methods for PM in stationary exhaust sources in China (GB/T 16157-1996) have not involved the collection of CPM; and the chemical composition of collected PM was quite different from that actually released into the atmosphere (Hu et al., 2016). The emission inventory constructed based on emission surveys did not include the CPM emissions. So it is important to introduce CPM emissions to the current emission inventory. For example, a European study improved OA simulations by including the CPM emissions from residential wood combustion sources (Van Der Gon et al., 2015). Morino et al. (2018) revised the emission inventory by the consideration of CPM in Japan and showed that the OA emission rates were up to seven times the previous ones and CPM contributed greatly to atmospheric OA concentrations. A shortcoming of that study was that it did not separate the effects of CPM emissions on POA and SOA concentrations. Moreover, studies still lack quantification of emissions of CPM released by stationary combustion sources in China.

In this study, we use the available CPM emission information to construct an emission inventory of CPM from stationary combustion and mobile sources in China (with a focus on OA) and conducted 15 sensitivity simulations to explore the contributions of CPM emissions to atmospheric OA and $PM_{2.5}$ concentrations during the winter haze episodes over China. This quantitative study about organic CPM emissions and the roles of CPM in the OA formation emphasizes the importance of constraining CPM emissions from stationary combustion and mobile sources.

2 Materials and methods

2.1 Estimations of CPM emissions

Table 1 explicitly states the definitions of some acronyms for better understanding. We collected available emission measurement data of CPM based on published literatures. Totally, CPM emission data from 52 stationary combustion sources were acquired (Table S3). The emission sectors for these data included coal-fired power plants, waste incineration power plants, industrial coal boilers, heavy oil boilers, wood boilers, natural gas boilers, diesel boilers, iron and steel plants, and incinerators. Emissions of CPM depend on many factors including source categories, fuel types, sampling flue gas temperature, and air pollution control devices (Feng et al., 2021). Also, different measurement methods produced different results of CPM emissions (Wang et al., 2020a). Recently, cooling and dilution methods have been applied to monitor CPM concentrations. CPM contained organic and inorganic fractions, but this study only focused on organic CPM emissions. The emission rate of organic CPM was estimated as follows in Eq. (1) and (2) (Morino et al., 2018):

$$E_{OM}(CPM) = \sum A \times EF_{OM}(CPM) = \sum A \times EF_{PM\,2.5}(FPM) \times \frac{EF_{OM}(CPM)}{EF_{PM\,2.5}(FPM)} \quad (1)$$

$$E_{OM}(CPM) = \sum E_{PM\,2.5}(FPM) \times \frac{C_{OM}(CPM)}{C_{PM\,2.5}(FPM)} \quad (2)$$

$$E_{OMsi}(CPM) = E_{OM}(CPM) \times \frac{E_{OMsi}(CPM)}{E_{OM}(CPM)} = E_{OM}(CPM) \times \frac{C_{OMsi}(CPM)}{C_{OM}(CPM)} \quad (3)$$

Where E_{OM} (CPM) is the emission rate of organic matter in CPM; EF_{OM} (CPM) is the emission factor of organic matter in CPM; $E_{PM2.5}$ (FPM) is the emission rate of $FPM_{2.5}$; $EF_{PM2.5}$ (FPM) is the emission factor of $FPM_{2.5}$; A denotes the activity level; C_{OM} (CPM) is the concentration of organic matter detected in CPM; and $C_{PM2.5}$ (FPM) is the detected concentration of $FPM_{2.5}$. A and $EF_{PM2.5}$ (FPM) in Eq. (1) were combined to calculate $E_{PM2.5}$(FPM) in Eq. (2), acquired from $PM_{2.5}$ emission rates in the emission inventory of baseline year. Among these parameters, C_{OM} (CPM) and $C_{PM2.5}$ (FPM) were derived from the collected emission survey data at the above stationary combustion sources. The ratios of C_{OM} (CPM) to C_{OM} (FPM) should be used to estimate E_{OM} (CPM), but due to the limited data and very low values of C_{OM} (FPM) at these stationary sources, $C_{PM2.5}$ (FPM) was used instead of C_{OM} (FPM). The ratios of E_{OM} (CPM) to $E_{PM2.5}$ (FPM) and EF_{OM} (CPM) to $EF_{PM2.5}$ (FPM) should be equal to the ratios of C_{OM} (CPM) to $C_{PM2.5}$ (FPM) at the same dilution ratio in the emission surveys. Table 2 summarizes the emission ratios of E_{OM} (CPM) to $E_{PM2.5}$ (FPM) for these stationary combustion sources. In this estimate, these emission ratios collected from the best available data were applied to represent the stationary combustion sources in the current emission inventory.

In addition, the component information of organic CPM is important to model the participation of organic CPM in atmospheric chemical reactions. The organic CPM mainly contains alkanes (with C_{10}-C_{30} being the major n-alkanes), esters, and polycyclic aromatic hydrocarbons (PAHs) (Li et al., 2017c, d; Song et al., 2020; Zheng et al., 2018). Based on the relationship between carbon number of n-alkanes and saturation concentrations (C^*) following Lu et al. (2018), it is reasonable to speculate that organic CPM is composed of organic matter which is semi-volatile (SVOCs, $10^0 \leqslant C^* \leqslant 10^3$ μg m^{-3}) or has intermediate volatility (IVOCs, $10^3 < C^* \leqslant 10^6$ μg m^{-3}), combined as OM_{si} (CPM). It denotes a collective term for a range of organic matter with different volatilities in CPM. Since the volatility characteristics of organic CPM from these stationary combustion sources have not been accurately determined in relevant measurement studies, the emissions of OM_{si} (CPM) were scaled to emissions of OM (CPM) in this estimate as shown in Eq. (3), that is, the total emissions of OM (CPM) were distributed in different volatility bins. E_{OMsi} (CPM) denotes the emission rate of OM_{si} in CPM; C_{OMsi} (CPM) denotes the concentration of OM_{si} in CPM. The specific partition coefficients for different volatility bins in the model will be discussed in the following Sect. 2.3. In addition to stationary sources, mobile sources also generate certain emissions of CPM. Due to the lack of CPM emission data from on-road and off-road vehicles, we increased OM emission rates of the transportation sector (TR) by 30% to consider the contributions of CPM from these mobile sources, following Morino et al. (2018) and Lu et al. (2020).

2.2 The model configuration

The three-dimensional Community Multiscale Air Quality (CMAQ, v5.3.2) model developed by the U.S. Environmental Protection Agency was used to simulate spatiotemporal distributions of chemical species. The detailed model configuration can refer to Appel et al. (2021) and Yu et al. (2014). The gas-phase chemical mechanism was based on the Carbon Bond Mechanism 6 (CB6) scheme. The aerosol module was based on the seventh-generation aerosol module of CMAQ (AERO7). The CMAQv5.0.2-VBS version with AERO6 coupled with a VBS module (AERO6VBS) was used for comparison. Compared to the SOA formation in AERO6 in the CMAQv5.2, the AERO7 module includes some improvements: enhanced consistency of the SOA formation pathways between chemical mechanisms based on CB and SAPRC, updated photooxidized monoterpene SOA yields (Xu et al., 2018), added uptake of water by hydrophilic organics (Pye et al., 2017), consumption of inorganic sulfate when forming isoprene epoxydiol organic sulfate (Pye et al., 2013), and replacement of the Odum two-product model with a VBS framework to parameterize SOA formation (Appel et al., 2021; Qin et al., 2021). Both

AERO6VBS and AERO7 contained five classes of organic matter with one class being nonvolatile and the other four classes being semi-volatile with effective saturation concentrations of 1, 10, 100, and 1000 μg m^{-3}. Each of these volatility bins was assigned to the CMAQ species of LVPO1, SVPO1, SVPO2, SVPO3 and IVPO1, respectively. The emissions of unspeciated IVOCs were set equal to 1.5 times the POA emissions in AERO6VBS and 6.579 times in AERO7 by default. The high scale factor of 6.579 in AERO7 was set to consider missing pathways for the SOA formation from combustion sources including the IVOCs oxidation (Murphy et al., 2017; Murphy et al., 2021), and it was primarily parameterized in Los Angeles where vehicle emissions are a principal source (Hayes et al., 2015). This parameter setting may not be suitable for fire and wood-burning sources, thus the scale factor was zeroed out for these sources in this study, as stated in the release of CMAQv5.3.2. Meteorological fields were predicted by the Weather Research and Forecasting (WRF) model version 3.7. The physical schemes of WRF were the same as those in Wu et al. (2018) and Zhang et al. (2021). Meteorological initial and boundary conditions were provided by the National Center for Environmental Prediction (NCEP) final analysis dataset with the spatial resolution of 1°×1° and temporal resolution of 6 h. The first several days were used for model spin-up, varied for different pollution periods as described in Sect. 2.4. The gridded anthropogenic emission data for 2014 and 2017 were derived from Emission Inventory of Air Benefit and Cost and Attainment Assessment System (EI-ABaCAS) developed by Tsinghua University (Dong et al., 2020; Zheng et al., 2019). It contained primary species such as $PM_{2.5}$, SO_2, NO_x, CO, NMVOCs, NH_3, BC, and OC from nine anthropogenic sectors (i.e., agriculture, power plant, industry process, industry combustion, steel, cement, residential, transport, and open burning). Biogenic source emissions were calculated by on-line Biogenic Emission Inventory System version 3.14 (BEISv3.14) model (Carlton and Baker, 2011). Dust emissions were calculated by an on-line windblown dust scheme (Choi and Fernando, 2008). Our study period in 2014 occurred before and during the Asia-Pacific Economic Cooperation (APEC) summit held in Beijing (November 5–11, 2014). During the period of pre-APEC (October 28–November 2) and full-APEC (November 3–11), some pollution control measures were gradually implemented in Beijing and its surrounding areas. Based on the observed reductions in the concentrations of $PM_{2.5}$, SO_2, NO_2, NO, and CO during APEC in Beijing and its surrounding cities (Li et al., 2017e, 2019; Wen et al., 2016), and 28% contribution of the emission control measures to the reduction of $PM_{2.5}$ concentrations (Liang et al., 2017), the approximate emission reduction of 30% was conducted during the above time period for the region of two municipalities (Beijing and Tianjin), four provinces (Hebei, Shanxi, Henan, and Shandong) and Inner Mongolia Autonomous Region. The simulation domain covered mainland China by

a 395 × 345 grid with the horizontal grid resolution of 12 km (Fig. 1). There were 29 vertical layers in σ_z coordinate system reaching the upper pressure (100 hPa) with 20 layers located in the lowest 3 km to resolve the planetary boundary layer.

2.3 Design of sensitivity simulation cases

According to the emission parameters summarized in Table 2, we carried out bootstrapping and Monte Carlo simulations to obtain the mean and uncertainty ranges of E_{OM} (CPM)/$E_{PM2.5}$ (FPM) for stationary combustion sources including power plant (PP), industry combustion (IN), and steel (IR) (see Table 3). First, the optimal probabilistic distributions and uncertainty ranges were determined for each source category. Then the statistical bootstrap simulation was applied to calculate the mean and 95% confidence interval of emission ratios for each source category. Finally, the uncertainties of these parameters were propagated to calculate the total uncertainty of emission by running Monte Carlo simulations for 10,000 times. Notably, the estimated uncertainties were only related to variabilities in the ratio of E_{OM}(CPM) to $E_{PM2.5}$(FPM), but did not necessarily represent the overall uncertainties of organic CPM emissions. On this basis, a series of sensitivity cases including low, medium, and high emission ratios were designed to explore the contributions of organic CPM emissions to OA concentrations and quantify uncertainty ranges of CPM effects on OA (see Table 4).

Here, to explore the contributions of organic CPM emissions to atmospheric OA and $PM_{2.5}$ concentrations, the estimated emissions of organic CPM were added into the CMAQ model as an individual source, separated from other emission sources. For the base scenarios, the simulations were performed with the inputs of the previous emission inventory without the newly constructed organic CPM emissions. Considering that organic FPM from stationary combustion and mobile sources mainly contained low volatile matter, all of these emissions should be assigned to the CMAQ species of LVPO1 and other volatility bins should be assigned a scale factor of 0, and the rests were kept at the default settings in the model. In addition, different volatility distributions could be chosen for different emission sources, but this was not our study focus and did not interfere with the results of CPM contributions. For the cases including CPM emissions from stationary combustion and mobile sources, the emissions of organic CPM were mapped to surrogate species for different volatility bins (LVPO1, SVPO1, SVPO2, SVPO3, and IVPO1) in the CMAQ model for representing the SOA formation from CPM. These mixed species underwent gas-particle partitioning and multi-generational gas-phase photochemical oxidation of organic vapors by OH radicals to generate successively lower volatility and more-oxygenated species,

and then produced SOA. Due to the unavailable volatility distribution information of OM_{si} (CPM), different scaling factors of volatility bins were employed under each emission scenario to discuss the uncertainties of CPM effects. In this study, we tested two kinds of scaling factors for the five volatility bins: fac1 (0.09, 0.09, 0.14, 0.18, 0.5) (Grieshop et al., 2009) and fac2 (0.40, 0.26, 0.40, 0.51, 1.43) (Shrivastava et al., 2011). As mentioned in Sect. 2.1, organic CPM was composed of organic matter which was semi-volatile or had intermediate volatility, thus the first bin which represents nonvolatile organic matter should be set to zero. Here, the original partition coefficient of the first bin was added to the following bin, so the fac1 (0, 0.18, 0.14, 0.18, 0.5) and fac2 (0, 0.66, 0.40, 0.51, 1.43) were applied in the sensitivity simulation cases. The fac2 estimated total SVOCs emissions as 3 times POA emissions to consider missing OM_{si} (CPM) emissions. Then the fac3 (0, 0.42, 0.27, 0.345, 0.965) which was the average of fac1 and fac2, was also tested for the five volatility bins. The fac1, fac2 and fac3 were applied to the OM_{si} (CPM) emissions for cases S1.1, S1.2 and S1.3, respectively (see Table 4). For an evaluation of the sensitivity of OA outputs to organic CPM emissions, we conducted simulations with different magnitudes of CPM emissions at the 95% and 50% confidence interval. Thus the S2-S3 cases were designed with the uncertainty ranges of E_{OM} (CPM)/$E_{PM2.5}$ (FPM) at 95% confidence interval (73% and 128% of the amounts in S1), and the S4-S5 cases with the uncertainty ranges at 50% confidence interval (90% and 109% of the amounts in S1). Moreover, the contributions of individual emission categories including PP, IN, IR, and TR were quantified by excluding perturbation of other sources in the S6-9 cases. The simulated contributions of CPM emissions to POA, SOA, OA, and $PM_{2.5}$ concentrations under these scenarios were calculated as the improved simulation concentrations after including CPM emissions relative to the base case, divided by the simulations under these scenarios.

2.4 Observational data

For the year 2014, the simulation period was from October 6 to November 14, 2014, with the first 8 days being the model spin-up time. Field observation data during the episode from October 14 to November 14, 2014, at the Institute of Atmospheric Physics (IAP) (39°58′ N, 116°22′ E) in Beijing were from Li et al. (2017a) and Xu et al. (2015). Concentrations of aerosol components were measured in PM_1. In order to make a comparison between simulated and observed results, the $PM_1/PM_{2.5}$ ratio of 0.77 was used to calculate the observed component concentrations in $PM_{2.5}$ based on the observations from Xu et al. (2015). To distinguish between SOA and POA, Aerosol Mass Spectrometer (AMS) measurements and the method of Positive Matrix Factorization (PMF) were used by Xu et al. (2015), identifying three POA

factors from coal combustion, biomass burning and cooking, and two SOA factors of semi-volatile and low-volatility oxygenated OA. Observation data of organic carbon (OC) on November 3, 2014, at Qianyanzhou (located in Jian city) and Changsha were provided by CERN Atmospheric Science Branch of the Institute of Atmospheric Physics, Chinese Academy of Sciences (Liu et al., 2018). For the year 2018, the simulation period was from December 1 to 31, 2018, with the first 5 days for model spin-up. The observation values of OC in the BTH2+26 cities were provided by China Environmental Monitoring Station. These cities include Beijing, Tianjin, Anyang, Baoding, Binzhou, Cangzhou, Changzhi, Dezhou, Hebi, Handan, Hengshui, Heze, Jincheng, Jinan, Jining, Jiaozuo, Kaifeng, Liaocheng, Langfang, Puyang, Shijiazhuang, Tangshan, Taiyuan, Xingtai, Xinxiang, Yangquan, Zibo, and Zhengzhou. The OA/OC ratio of 1.4 (Simon et al., 2011) was used to calculate OA concentrations for the comparison with the simulation results. The observed concentrations of $PM_{2.5}$ were collected from the Chinese National Environmental Monitoring Center (CNEMC). Since the $PM_{2.5}$ observation data from December 22 to 26 were missing, the following analysis of $PM_{2.5}$ did not include these five days. The hourly observation data of meteorological factors, including temperature (T), relative humidity (RH), wind speed (WS), and wind direction (WD), were provided by the China Meteorological Administration (http://data.cma.cn/site/index.html).

3 Results and discussion

3.1 Emissions of condensable particulate matter

Emissions of OM in CPM (E_{OM}(CPM)) were comparable to or even exceeded the emissions of filterable $PM_{2.5}$ ($E_{PM2.5}$(FPM)) for most stationary combustion sources, regardless of the differences among these values (Table 2). Therefore, we constructed a new emission inventory by including CPM. The annual emissions of OA in previous and modified emission inventory over China for the year 2014 and 2017 are presented in Fig. 2. The OM represents the organic matter in the emission input before the further volatility distributions, while OM (C^*≤100 μg m^{-3}) represents the organic matter allocated in the bin of C^* equal to 100 and below after application of the volatility distributions for the fac1, fac2 and fac3 cases. Based on the simulation case settings, OM (FPM) from all the sectors was multiplied by fac1 (0.5), while OM (CPM) from stationary combustion and mobile sources was multiplied by fac1 (0.5), fac2 (1.57) or fac3 (1.035). In the previous inventory for 2014 without CPM, the emissions of OM over mainland China were 3664.6 Gg, approximately equal to 40% of $PM_{2.5}$ emissions. After the inclusion of CPM released by stationary combustion sources in the new inventory, the emissions of OM were

enhanced by a factor of 2 and even exceeded emissions of $FPM_{2.5}$. The dominant contributors of OM (FCPM) are combustion sources in power plant and industrial sectors, estimated to be 66% (7006.2 Gg) of the total OA emissions (10531.1Gg). The emissions of OM (C^*≤100 μg m^{-3}) remained unchangeable for the open burning, domestic, and industry process sources since they were mostly FPM, while OM (C^*⩽100 μg m^{-3}) for the power plant, industry combustion, and steel sources were variable based on whether fac1, fac2 or fac3 were applied to the CPM. Similarly, the emissions of OM (FCPM) were 3 times those of OM (FPM) for the year 2017. The emissions of OM from power plant, industry combustion, and steel sources increased by 33 times after considering CPM emissions. These results indicate that the inclusion of organic CPM from stationary combustion sources has a major impact on OM emissions and improves contributions of industrial and power sectors to OM emissions.

Notably, the emission estimates of OM in CPM contained uncertainties, mainly attributed to the representativeness and limitations of chosen emission sources. For power plant, industry combustion, and steel sectors, the average ratios of E_{OM} (CPM) to $E_{PM2.5}$ (FPM) were 4.12, 1.38 and 2.80, respectively (Table 3). The estimation of uncertainties related to variabilities in the ratio of E_{OM} (CPM) to $E_{PM2.5}$ (FPM) was described in section 2.3. Overall, the uncertainty range of E_{OM} (CPM) related to variabilities in the ratio was -27% ~ +28% at the 95% confidence interval. On this basis, a series of sensitivity cases with different emission ratios were set to determine the uncertainty ranges of CPM contributions (Table 4). In the future, actual measurements of organic CPM emissions from various sources and source-specific identification of volatility distributions are needed to reduce uncertainties in emission estimates.

3.2 Effects of CPM emissions on POA and SOA concentrations

For the hourly observed and simulated SOA and POA concentrations at the Beijing site, Figs. 3 and 4 show obvious improvements of SOA and POA levels after the consideration of CPM contributions. The specific model species for POA and SOA are shown in Table S4. In all the simulation scenarios, five complete ascending and descending SOA episodes in Fig. 3 were well captured, with much lower mean bias between observations and simulations than previous results of Li et al. (2017a). Three pollution episodes before the APEC were clearly captured by the model. The third episode (October 27–November 1) had lower observed SOA levels relative to the first (October 16–21) and second episodes (October 22–26), attributed to lower precursor emission concentrations, lower temperature, and regional transports by strong northerly winds on October 26. During the APEC, there were two pollution episodes with lower SOA concentrations due to the effects of emission controls and meteorological conditions (Ansari et al.,

2019; Liang et al., 2017). Compared to the observed values, cases without CPM exhibited varying degrees of underestimation for SOA and POA. For example, in the base case, the maximum SOA values were underestimated by 50% in the first episode and up to 65% in the second episode, while the simulated hourly POA values varied in the range of 0.12~19.06 μg m^{-3}, much lower than POA observations during the whole time period. In comparison, the AERO6VBS case underpredicted SOA by up to 65%, and simulated low levels of POA during the first three periods and high levels in the last two episodes. Overall, the base case underestimated the average POA, SOA and OA levels by 74%, 56% and 65% (Table 5), respectively, emphasizing the potential contributions of missing CPM sources.

After considering organic CPM emissions, the underestimation of average POA and SOA was reduced to 37% and 15% under the S1.1 scenario, respectively (Table 5). From the simulated hourly variations in the S1.1 case (Fig. 3), SOA concentrations were enhanced by factors of 0.01~1.86 relative to base case, more consistent with the observations. The gap between average simulations and observations decreased from -9.84 to -2.61 μg m^{-3} (73% decrease). For the peak values in the first, second, fourth, and fifth pollution episodes, the improvements in the peak SOA concentrations were approximately 30, 30, 10, and 15 μg m^{-3}. Nevertheless, the overestimation of SOA occurred in the third process, mainly due to meteorological conditions considering the fact that the observed and modeled wind directions were inconsistent during this period as shown in Fig. S1. The prevailing southerly and northeast wind directions in the model during the third process did not bring clean air from the northwest boundary to dilute the local generated SOA (Li et al., 2016, 2019). Also, higher simulated wind speeds transported more precursors with the southerly and northeast winds and caused the overestimation of SOA (see Fig. S1). Correspondingly, the hourly POA simulation concentrations in the S1.1 case increased by 0.07~3.70 times compared to the base case, narrowing the average gap between simulations and observations from -11.97 to -6.01 μg m^{-3} (50% decrease), but the high observed levels of POA were still not attained under this scenario. Comparatively, the S1.2 case presented similar hourly simulation results of SOA to the S1.1 case with the enhancement by factors of 0.02~2.21 versus the base case, while the simulated POA values were nearly 1.3 times higher than the S1.1 case, capturing most of the high observations throughout the whole study period. Under the S1.3 scenario using different SVOCs parameters from the S1.1 case, the simulation concentrations of SOA were 4% higher and POA were 61% higher than those under the S1.1 scenario as shown in Table 5. Based on the evaluation results, the S1.3 scenario showed the optimal improvement effects, with the mean biases of 1.23% for POA and -11.68% for SOA (see Table 5). In consideration of the uncertainty ranges of CPM emissions, a series of sensitivity cases with different

emission ratios were conducted. Under the minimum emission scenario in the S2.1 case, the average SOA and POA concentrations were 12%, and 15% lower than those in the S1.1 case, respectively. Under the maximum emission scenario in the S3.1 case, the average SOA and POA concentrations were 14% and 19% higher than those in the S1.1 case, respectively. Thus the model can resolve 63% (54%~75%) of the observed POA concentrations and 85% (75%~97%) of the observed SOA concentrations in the cases S1.1 (S2.1, S3.1). Then the S2.2 and S3.2 cases applied the same S/IVOCs parameters as S1.2, and also displayed similar results of SOA to those in the S2.1 and S3.1 cases, respectively. Under this setting, the uncertainty ranges were -13% to +13% for SOA, and -22% to +24% for POA in the S1.2 case as shown in Table 5. For the S4.2 and S5.2 cases with the CPM emissions at 50% confidence interval, their SOA concentrations showed small changes with 5% lower in the S4.2 case and 4% higher in the S5.2 case than the S1.2 case; similar minor sensitivity of 8% decrease (S4.2) and 7% increase (S5.2) were found for POA. To explore the contribution of each source category to SOA and POA and identify the key anthropogenic sources of CPM, we conducted simulations with the different separate inputs (S6~S9) (see Table 4). Results show that the CPM emissions from the IR sector made the largest contribution to the POA and SOA increases, accounting for 59% of POA and 55% of SOA, followed by PP (26% for POA and 30% for SOA) and IN sources (13% for POA and 14% for SOA). This was consistent with the differences in the CPM emissions from the above three source sectors (Fig. 2). The sensitivities of SOA and POA to the emission ratio of organic CPM from the TR sector were very small, indicating a weak impact on OA due to small contributions of transportation sources to the OA emissions in FCPM. The above results demonstrate that CPM from stationary sources was an important source for both POA and SOA formations. In summary, when considering the uncertainties of organic CPM emissions, CPM can be a significant contributor to OA concentrations, with the contributions of 58% (51%, 65%) to POA, 49% (42%, 55%) to SOA, 53% (45%, 59%) to OA under the S1.1 (S2.1, S3.1) scenario, and 82% (76%, 85%) to POA, 53% (45%, 58%) to SOA, 70% (63%, 75%) to OA under the S1.2 (S2.2, S3.2) scenario. The S1.3 scenario had the best improvement performance with CPM contributing 74% to POA, 51% to SOA, and 63% to OA.

Because of the better representations of temporal variations of SOA and POA after including CPM emissions, OA simulations were correspondingly improved. To separate the effects of CPM on OA into different process contributions, we compared simulation results of these sensitivity cases as shown in Fig. 5. The OA composition contains POA, ASOA (SOA from anthropogenic VOCs), BSOA (SOA from biogenic VOCs), and SISOA (SOA from S/IVOCs). The difference between simulations and observations

decreased from 21.81 μg m^{-3} in the base case to 8.63 μg m^{-3} in the S1.1 case (60% decrease), with the uncertainty of 11.92 μg m^{-3} (45% decrease in S2.1) to 4.66 μg m^{-3} (79% decrease in S3.1) relative to the base case. However, these cases still underestimated the observed OA levels. The S1.2, S2.2 and S3.2 cases increased the contributions of CPM to OA by 14.01, 10.24, 17.92 μg m^{-3} compared to S1.1, S2.1 and S3.1, respectively. Notably, the average OA simulations in S1.3 were relatively close to the observations, with the average CPM contributions of 19.98 μg m^{-3} and a minor underestimation of 5.43% (see Table 5). Taking OA composition into account, POA and SISOA accounted for the largest part in all these scenarios. The effects of CPM were only reflected in the enhancements of POA and SISOA. These results suggest that OA was sensitive to the emissions of organic CPM, so it is required to reduce emission uncertainties for better simulations. To sum up, the revised simulations after the inclusion of CPM from stationary combustion and mobile sources led to improved modeling performances of OA during the winter haze episodes, revealing a significant contribution of CPM to atmospheric OA.

3.3 Effects of CPM on OA and $PM_{2.5}$ concentrations

To ensure the accuracy and reliability of our modeling results, further studies in other cities were presented. Fig. 6 shows large contributions of CPM to OA on November 3, 2014, at Changsha and Qianyanzhou. After the inclusion of CPM effects in the S1.1, S1.2 and S1.3 cases versus the base case, the simulated OA concentrations were improved by 6.28, 15.80 and 9.60 μg m^{-3} for Changsha, respectively. The simulated OA concentrations increased by 7.06, 15.28 and 10.14 μg m^{-3} in the S1.1, S1.2 and S1.3 cases versus the base case for Qianyanzhou, respectively. Comparatively, the S1.2 case contributed to greater increases of OA concentrations, narrowing the simulation-observation bias from 79% to less than 40% for Changsha and more than 70% to less than 25% for Qianyanzhou. The remaining bias was probably attributed to the underestimation of our estimated CPM emissions, effects of meteorological factors and other missing SOA formation pathways.

The impacts of CPM on OA were studied during December 6–30, 2018, in the BTH 2+26 cities. Likewise, the improvements in daily OA simulation concentrations can be found at the four studied cities after the consideration of CPM, especially for high pollution days (Fig. 7). The modeled underestimations of OA were improved from -60.88% to -22.55%, -56.47% to -7.91%, -68.38% to -30.51%, and -62.84% to -24.99% with the inclusion of CPM emissions in the S1.1 case relative to the base case for Handan, Shijiazhuang, Xingtai and Dezhou, respectively (Table 5). The contributions of CPM emissions to total OA concentrations reached up to 49%, 53%, 54%, and 50% for Handan, Shijiazhuang, Xingtai, and

Dezhou, respectively. Under the S1.3 scenario, the OA simulations showed greater increases, and slightly exceeded observation values with the mean biases of 8.00%, 37.42%, 0.81%, and 2.21% for the above four cities, respectively. For example, daily OA levels in Handan increased by 5.60~57.89 μg m^{-3} after including CPM effects (S1.1 versus base case). On average, the inclusion of CPM doubled the OA concentrations. However, some observations were not captured, while the observed value on December 20 was overestimated, indicating uncertainties of the estimated organic CPM emissions. Under the S1.3 scenario, the average simulated OA concentrations were enhanced by 1.8 times relative to the base case, with a good capture of some underestimated values in the S1.1 case. For Shijiazhuang with daily OA concentrations below 80 μg m^{-3}, the base case underestimated OA levels by 12~78%. After incorporating the CPM emissions in the S1.1 case, the daily OA concentrations were significantly improved by factors of 0.7~1.7. Some observed high values of OA were well captured in the S1.1 case on December 10 with the simulation of 67.75 μg m^{-3} versus observation of 58.65 μg m^{-3}, and on December 14 and 30. Under the S1.3 scenario, the daily OA levels increased by factors of 1.3~3.6 relative to the base case. Although the average OA concentrations were somewhat overestimated in the S1.3 case, good agreements between observations and simulations existed on some days, including December 9, 12, 13, 16-19, and 24. For Xingtai, the simulated OA concentrations were enhanced by factors of 1.0~1.8 in the S1.1 case relative to the base case. The model can resolve 69% of average OA observations in the S1.1 case when the emissions of CPM were included. The average OA simulation value was improved by 29.21 μg m^{-3} in the S1.3 case compared to the base case. Then Dezhou showed similar results with the enhancement of 0.7~1.6 times for daily OA contributed by CPM in S1.1. Although the observed high OA concentrations exceeding 80 μg m^{-3} on December 11 and 16 were not captured in the S1.1 case, the bias between simulation and observation was reduced to -21.92 and -25.63 μg m^{-3} versus -59.17 and -52.64 μg m^{-3} in the base case, respectively. The underestimations of high OA levels on December 11 and 16 were resolved in the S1.3 case, and the average concentration over the whole period was very close to the observation. Table S2 shows the model evaluation results for $PM_{2.5}$ concentrations under different sensitivity simulation cases. Dezhou was not included due to the missing data. After including the CPM emissions in the S1.1 case, the model can resolve 86%, 86%, and 72% of average $PM_{2.5}$ observations with increases in $PM_{2.5}$ concentrations by 32%, 37%, and 38% relative to the base case for Handan, Shijiazhuang, and Xingtai, respectively. $PM_{2.5}$ simulations were further enhanced for these four cities in the S1.3 case with the NMB values of 2.04%, 7.21%, and -12.08%, respectively. It was notable that the emissions of inorganic components in CPM were not investigated in this study, which can cause modeling deviation.

Other factors including boundary layer height and wind can also affect the simulations. In summary, our estimated CPM emissions showed a reasonable range, which can make a significant contribution to atmospheric OA and $PM_{2.5}$.

3.4 Regional contributions of CPM to OA and $PM_{2.5}$

The regional effects of CPM emissions on atmospheric OA and $PM_{2.5}$ from a nationwide perspective were investigated. The concentrations of POA, SOA and OA averaged over the whole study period from October 14 to November 14, 2014, showed varying degrees of regional increases after incorporating CPM emissions, mainly in central and eastern regions in China (Fig. 8). In the base case, the simulation values of POA and SOA were both lower than 14 μg m^{-3} over China. Correspondingly, OA concentrations did not exceed 22 μg m^{-3} with the maximum values distributed in the BTH region and Central China. After the consideration of CPM effects in the S1.1 case relative to the base case, the concentrations of POA, SOA and OA substantially increased over North China, East China, and Central China including Beijing, Tianjin, Shanghai, and provinces of Liaoning, Shandong, Shanxi, Henan, Hubei, Anhui, Jiangsu, Zhejiang, Hunan, Jiangxi. The most remarkable enhancement values were up to 10, 12, and 20 μg m^{-3} for POA, SOA and OA, respectively. Then under the S1.2 scenario with the same emissions as the S1.1 case but different SIVOCs parameterization, substantial increases in the POA simulations by more than 16 μg m^{-3} were found for most cities in North China, East China, and Central China, with the maximum distributed in the BTH region (up to 24 μg m^{-3}), attributable to large amounts of emissions from industrial plants and power plants in this region. The OA concentrations for many cities located in North China and East China increased by more than 24 μg m^{-3} after including CPM emissions in the S1.2 case. Since the contributions of CPM to SOA in the S1.2 case were only slightly larger than those in the S1.1 case, the greater improvements of OA in S1.2 mainly result from the POA increases. The regional increases in the POA, SOA and OA simulations in the S1.3 case were not lower than 10, 8, and 18 μg m^{-3} for most cities in North China, East China, and Central China, respectively.

The regional contributions of organic CPM emissions to $PM_{2.5}$ concentrations were explored in the BTH2+26 cities averaged over the period from December 6 to 30, 2018 (Fig. 9). In the base case without the CPM effects, the model comparisons against observations suggest that $PM_{2.5}$ levels were greatly underestimated in almost all cities except Tangshan (Fig. 9a). Several cities with observed $PM_{2.5}$ concentrations higher than 80 μg m^{-3} showed the greatest underestimations with simulation values under 50 μg m^{-3}. Under the S1.1 scenario including CPM emissions, the simulated $PM_{2.5}$ concentrations were

substantially enhanced in almost all the studied cities, closer to the observations (Fig. 9b). The contributions of CPM to $PM_{2.5}$ were not lower than 14 μg m^{-3} for the most cities (Fig. 9c). Under the S1.3 scenario, CPM made a significant contribution to $PM_{2.5}$ concentrations, more than 24 μg m^{-3} for most cities (Fig. 9f). High observations for Baoding, Shijiazhuang, Xingtai, Hengshui, Dezhou and Handan were well captured (Fig. 9e). The scatter plots of observed and simulated daily $PM_{2.5}$ concentrations for all BTH2+26 cities in Fig. 9d show obvious improvement in $PM_{2.5}$ simulations after including CPM emissions, with the NMB values from -32.4% in the base case to -10.6% in the S1.1 case, and then to 5.5% in the S1.3 case. Nevertheless, there were still model-measurement biases for $PM_{2.5}$ concentrations in some cities with high observations exceeding 90 μg m^{-3}, including Baoding, Anyang, Puyang, Heze, Zhengzhou and Kaifeng. The insufficient improvement of $PM_{2.5}$ can be attributed to incomplete emission information of inorganic components, which need further research. In addition, some heavy pollution hours were chosen to investigate the regional impacts of CPM on $PM_{2.5}$ concentrations, including 8:00, 9:00, 10:00, 11:00, and 21:00 on December 15 (Fig. 10a). Besides the BTH2+26 cities, some surrounding cities (Chaoyang, Chengde, Datong, Dongying, Huludao, Jinzhou, Linxi, Luoyang, Luohe, Qinhuangdao, Qindao, Rizhao, Sanmenxia, Shangqiu, Shuozhou, Taian, Weihai, Weifang, Xinzhou, Xinyang, Yantai, Zaozhuang, Zhangjiakou, Zhoukou, Zhunmadian) were also included. Results show that the underestimated $PM_{2.5}$ concentrations in the base case were substantially improved after considering CPM emissions in S1.1 and S1.3, especially for some high observations over 170 μg m^{-3}. Better agreement between simulated and observed $PM_{2.5}$ concentrations for all these cities was achieved, with the NMB values from -32.6% in the base case to -12.3% in S1.1, and to 0.6% in S1.3 (Fig. 10b). To sum up, the consideration of CPM effects can improve the underestimation of regional OA and $PM_{2.5}$ simulations to a certain extent, especially during the heavy pollution periods.

4 Conclusions

In this study, we focused on emissions of condensable PM from stationary combustion and mobile sources and developed an emission inventory of organic CPM in China. Using emission inputs with and without CPM contributions, the CMAQ model was applied to simulate the impacts of CPM on atmospheric OA and $PM_{2.5}$ in China. The results show that the inclusion of CPM emissions increased annual OA emissions by a factor of 2 for both the years 2014 and 2017. The power plant, industry combustion, and steel sectors in the stationary combustion sources dominated OA emissions in the new inventory. A series of sensitivity scenarios with different emission ratios and volatility distributions show

that CPM contributed significantly to the improvement of hourly SOA and POA concentrations during the period from October 14 to November 14, 2014, at Beijing. The contributions of CPM were 51 ~ 85% to POA and 42 ~ 58% to SOA under these scenarios. The model comparison against observations suggests that the consideration of CPM effects improved the underestimations of simulation results and achieved a good capture of peak SOA and POA values. In addition, the enhancements of daily OA levels by CPM were demonstrated during December 6-30, 2018 at Handan, Shijiazhuang, Xingtai and Dezhou. Compared to daily observations, the NMB values in these four cities were improved from -60.88%, -56.47%, -68.38%, -62.84% (the base case) to -22.55%, -7.91%, -30.51%, -24.99% (the S1.1 case) for POA, SOA and OA, respectively. The regional contributions of CPM also narrowed the gap between simulated and observed concentrations of $PM_{2.5}$ in the BTH2+26 cities. In conclusion, our estimated CPM emissions contributed significantly to the improvements of simulation performances for both atmospheric OA and $PM_{2.5}$, especially during the high pollution episodes. Therefore, the CPM emissions can be incorporated into chemical transport models together with FPM to improve the simulation accuracies of OA and $PM_{2.5}$.

Our estimates of organic CPM emissions and SOA formation from CPM contained the following uncertainties: (1) The construction of the organic CPM emission inventory in the present study was based on the ratios of E_{POA}(CPM) to $E_{PM2.5}$(FPM) derived from limited sources, instead of the actual measurement data of CPM emissions from the different sources and regions over China. (2) Since there was no explicit volatility characterization of primary organic CPM species available for incorporation into the emission inventories, the S/IVOCs emissions were scaled to the POA emissions. (3) Due to the lack of relevant data, the original surrogate species of S/IVOCs and their properties in the CMAQ model remained unchanged for representing the SOA formation from CPM, rather than introducing new model species with identified parameters related to OH reaction rates, effective saturation concentration, and multigenerational aging products. Based on these limitations, it is strongly recommended that future studies conduct extensive surveys of CPM emissions from various stationary combustion sources and measure the actual emissions of source-specific and region-specific S/IVOCs to better constrain OA simulations by chemical transport models.

Data availability. The emission data and model results are available upon request.

Supplement. The supplement related to this article is available online.

Author contributions. S.Y., P.L. conceived and designed the research. M. L. performed model simulations.

M. L., X. C., Y. Z., and Z. L. conducted data analysis. Z. S., W. L., X. Z, B. N. M., K. A., R. M., D. R., and J. H. S contributed to the scientific discussions. M. Z, Y. S., Z. L., and C. S. provided observation data. S. W. provided the Abacas emission data. S. Y., M. L, P. L., and J. H. S wrote and revised the manuscript.

Competing interests. The authors declare that they have no conflict of interest.

Disclaimer. The views expressed in this article are those of the authors and do not necessarily represent the views or policies of the U.S. Environmental Protection Agency.

Acknowledgements. The authors would like to thank Comprehensive data collection and sharing platform for atmospheric environmental science (https://napcdata.craes.cn), and CERN Atmospheric Science Branch of the Institute of Atmospheric Physics, Chinese Academy of Sciences for providing OC measurement data.

Financial support. This study is supported by the National Natural Science Foundation of China (No. 42175084, 21577126, 41561144004, and 92044302), Department of Science and Technology of China (No. 2018YFC0213506 and 2018YFC0213503), and National Research Program for Key Issues in Air Pollution Control in China (No. DQGG0107). Pengfei Li is supported by National Natural Science Foundation of China (No. 22006030), Initiation Fund for Introducing Talents of Hebei Agricultural University (412201904), and Hebei Youth Top Fund (BJ2020032).

References

Ansari, T. U., Wild, O., Li, J., Yang, T., Xu, W., Sun, Y. and Wang, Z.: Effectiveness of short-term air quality emission controls: a high-resolution model study of Beijing during the Asia-Pacific Economic Cooperation (APEC) summit period, Atmos. Chem. Phys., 19(13), 8651–8668, doi:10.5194/acp-19-8651-2019, 2019.

Appel, K. W., Bash, J. O., Fahey, K. M., Foley, K. M., Gilliam, R. C., Hogrefe, C., Hutzell, W. T., Kang, D., Mathur, R., Murphy, B. N., Napelenok, S. L., Nolte, C. G., Pleim, J. E., Pouliot, G. A., Pye, H. O. T., Ran, L., Roselle, S. J., Sarwar, G., Schwede, D. B., Sidi, F. I., Spero, T. L. and Wong, D. C.: The Community Multiscale Air Quality (CMAQ) model versions 5.3 and 5.3.1: System updates and evaluation, Geosci. Model Dev., 14(5), 2867–2897, doi:10.5194/gmd-14-2867-2021, 2021.

Carlton, A. G. and Baker, K. R.: Photochemical modeling of the ozark isoprene volcano: MEGAN, BEIS, and their impacts on air quality predictions, Environ. Sci. Technol., 45(10), 4438–4445, doi:10.1021/es200050x, 2011.

Carlton, A. G., Wiedinmyer, C. and Kroll, J. H.: A review of Secondary organic aerosol (SOA) formation from isoprene, Atmos. Chem. Phys., 9(14), 4987–5005, doi:10.5194/acp-9-4987-2009, 2009.

Chen, L., Zhu, J., Liao, H., Gao, Y., Qiu, Y., Zhang, M., Liu, Z., Li, N. and Wang, Y.: Assessing the formation and evolution mechanisms of severe haze pollution in the Beijing-Tianjin-Hebei region using process analysis, Atmos. Chem. Phys., 19(16), 10845–10864, doi:10.5194/acp-19-10845-2019, 2019.

Choi, Y. J. and Fernando, H. J. S.: Implementation of a windblown dust parameterization into MODELS-3/CMAQ: Application to episodic PM events in the US/Mexico border, Atmos. Environ., 42(24), 6039–6046, doi:10.1016/j.atmosenv.2008.03.038, 2008.

Corio, L.A., Sherwell, J.: In-stack condensible particulate matter measurements and issues. J. Air Waste Manage. Assoc.

50, 207–218, 2000.
Donahue, N. M., Robinson, A. L., Stanier, C. O., and Pandis, S. N.: Coupled partitioning, dilution, and chemical aging of semivolatile organics, Environ. Sci. Technol., 40, 2635–2643, https://doi.org/10.1021/es052297c, 2006.
Donahue, N. M., Epstein, S. A., Pandis, S. N., and Robinson, A. L.: A two-dimensional volatility basis set: 1. organic-aerosol mixing thermodynamics, Atmos. Chem. Phys., 11, 3303–3318, https://doi.org/10.5194/acp-11-3303-2011, 2011.
Dong, Z., Wang, S., Xing, J., Chang, X., Ding, D. and Zheng, H.: Regional transport in Beijing-Tianjin-Hebei region and its changes during 2014–2017: The impacts of meteorology and emission reduction, Sci. Total Environ., 737, 139792, doi:10.1016/j.scitotenv.2020.139792, 2020.
EPA, United States Environmental Protection Agency, Method 202 A – Dry Impinger Method for Determining Condensable Particulate Emissions from Stationary Sources, 2017.
Feng, Y., Li, Y., Cui, L.: Critical review of condensable particulate matter, Fuel, 224, 801–813, 2018.
Feng, Y., Li, Y., Zhang, X., Su, S., Zhang, Z., Gan, Z. and Dong, Y.: Comparative study on the characteristics of condensable particulate matter emitted from three kinds of coal, Environ. Pollut., 270, 116267, doi:10.1016/j.envpol.2020.116267, 2021.
Fu, T. M., Cao, J. J., Zhang, X. Y., Lee, S. C., Zhang, Q., Han, Y. M., Qu, W. J., Han, Z., Zhang, R., Wang, Y. X., Chen, D. and Henze, D. K.: Carbonaceous aerosols in China: Top-down constraints on primary sources and estimation of secondary contribution, Atmos. Chem. Phys., 12(5), 2725–2746, doi:10.5194/acp-12-2725-2012, 2012.
Fuzzi, S., Andreae, M. O., Huebert, B. J., Kulmala, M., Bond, T. C., Boy, M., Doherty, S. J., Guenther, A., Kanakidou, M., Kawamura, K., Kerminen, V. M., Lohmann, U., Russell, L. M. and Pöschl, U.: Critical assessment of the current state of scientific knowledge, terminology, and research needs concerning the role of organic aerosols in the atmosphere, climate, and global change, Atmos. Chem. Phys., 6(7), 2017–2038, doi:10.5194/acp-6-2017-2006, 2006.
Gao, M., Carmichael, G. R., Wang, Y., Saide, P. E., Yu, M., Xin, J., Liu, Z. and Wang, Z.: Modeling study of the 2010 regional haze event in the North China Plain, Atmos. Chem. Phys., 16(3), 1673–1691, doi:10.5194/acp-16-1673-2016, 2016.
Gehring, U., Gruzieva, O., Agius, R. M., Beelen, R., Custovic, A., Cyrys, J., Eeftens, M., Flexeder, C., Fuertes, E., Heinrich, J., Hoffmann, B., de Jongste, J. C., Kerkhof, M., Klümper, C., Korek, M., Mölter, A., Schultz, E. S., Simpson, A., Sugiri, D., Svartengren, M., von Berg, A., Wijga, A. H., Pershagen, G. and Brunekreef, B.: Air pollution exposure and lung function in children: The ESCAPE project, Environ. Health Perspect., 121(11–12), 1357–1364, doi:10.1289/ehp.1306770, 2013.
Van Der Gon, H. A. C. D., Bergström, R., Fountoukis, C., Johansson, C., Pandis, S. N., Simpson, D. and Visschedijk, A. J. H.: Particulate emissions from residential wood combustion in Europe - revised estimates and an evaluation, Atmos. Chem. Phys., 15(11), 6503–6519, doi:10.5194/acp-15-6503-2015, 2015.
Grieshop, A. P., Logue, J. M., Donahue, N. M. and Robinson, A. L.: Laboratory investigation of photochemical oxidation of organic aerosol from wood fires 1: measurement and simulation of organic aerosol evolution, Atmos. Chem. Phys., 9, 1263–1277, 2009.
Han, Z., Xie, Z., Wang, G., Zhang, R. and Tao, J.: Modeling organic aerosols over east China using a volatility basis-set approach with aging mechanism in a regional air quality model, Atmos. Environ., 124, 186–198, doi:10.1016/j.atmosenv.2015.05.045, 2016.
Hayes, P. L., Carlton, A. G., Baker, K. R., Ahmadov, R., Washenfelder, R. A., Alvarez, S., Rappenglück, B., Gilman, J. B., Kuster, W. C., De Gouw, J. A., Zotter, P., Prévôt, A. S. H., Szidat, S., Kleindienst, T. E., Offenberg, J. H., Ma, P. K. and Jimenez, J. L.: Modeling the formation and aging of secondary organic aerosols in Los Angeles during CalNex 2010, Atmos. Chem. Phys., 15(10), 5773–5801, doi:10.5194/acp-15-5773-2015, 2015.
He, X., Wang, Q., Huang, X. H. H., Huang, D. D., Zhou, M., Qiao, L., Zhu, S., Ma, Y. ge, Wang, H. li, Li, L., Huang, C., Xu, W., Worsnop, D. R., Goldstein, A. H. and Yu, J. Z.: Hourly measurements of organic molecular markers in urban Shanghai, China: Observation of enhanced formation of secondary organic aerosol during particulate matter episodic periods, Atmos. Environ., 240, doi:10.1016/j.atmosenv.2020.117807, 2020.
Hu, Y., Feng, Y., Wang, C., Ma, Z. and Jiang, T.: Studies on Monitoring Method of Condensable Particulate and Water-

soluble Ions in Fumes from Coal Fired Boilers, Environ. Monit. Manag. Technol., 28(1), 41–45, 2016.
Huang, R. J., Zhang, Y., Bozzetti, C., Ho, K. F., Cao, J. J., Han, Y., Daellenbach, K. R., Slowik, J. G., Platt, S. M., Canonaco, F., Zotter, P., Wolf, R., Pieber, S. M., Bruns, E. A., Crippa, M., Ciarelli, G., Piazzalunga, A., Schwikowski, M., Abbaszade, G., Schnelle-Kreis, J., Zimmermann, R., An, Z., Szidat, S., Baltensperger, U., El Haddad, I. and Prévôt, A. S. H.: High secondary aerosol contribution to particulate pollution during haze events in China, Nature, 514(7521), 218–222, doi:10.1038/nature13774, 2015.
Huang, X., Ding, A., Gao, J., Zheng, B., Zhou, D., Qi, X., Tang, R., Wang, J., Ren, C., Nie, W., Chi, X., Xu, Z., Chen, L., Li, Y., Che, F., Pang, N., Wang, H., Tong, D., Qin, W., Cheng, W., Liu, W., Fu, Q., Liu, B., Chai, F., Davis, S. J., Zhang, Q. and He, K.: Enhanced secondary pollution offset reduction of primary emissions during COVID-19 lockdown in China, Natl. Sci. Rev., 8(2), doi:10.1093/nsr/nwaa137, 2021.
Jathar, S. H., Woody, M., Pye, H. O. T., Baker, K. R. and Robinson, A. L.: Chemical transport model simulations of organic aerosol in southern California: Model evaluation and gasoline and diesel source contributions, Atmos. Chem. Phys., 17(6), 4305–4318, doi:10.5194/acp-17-4305-2017, 2017.
Kanakidou, M., Seinfeld, J. H., Pandis, S. N., Barnes, I., Dentener, F. J., Facchini, M. C., Van Dingenen, R., Ervens, B., Nenes, A., Nielsen, C. J., Swietlicki, E., Putaud, J. P., Balkanski, Y., Fuzzi, S., Horth, J., Moortgat, G. K., Winterhalter, R., Myhre, C. E. L., Tsigaridis, K., Vignati, E., Stephanou, E. G. and Wilson, J.: Organic aerosol and global climate modelling: A review, Atmos. Chem. Phys., 5(4), 1053–1123, doi:10.5194/acp-5-1053-2005, 2005.
Kroll, J. H. and Seinfeld, J. H.: Chemistry of secondary organic aerosol: Formation and evolution of low-volatility organics in the atmosphere, Atmos. Environ., 42(16), 3593–3624, doi:10.1016/j.atmosenv.2008.01.003, 2008.
Lane, T. E., Donahue, N. M. and Pandis, S. N.: Simulating secondary organic aerosol formation using the volatility basis-set approach in a chemical transport model, Atmos. Environ., 42(32), 7439–7451, doi:10.1016/j.atmosenv.2008.06.026, 2008.
Li, P. F., Yan, R. C., Yu, S. C., Wang, S., Liu, W. P., and Bao, H. M.: Reinstate regional transport of PM2.5 as a major cause of severe haze in Beijing, Proc Natl Acad Sci USA (PNAS), 112(21), E2739–E2740. doi:10.1073/pnas.1502596112., 2015.
Li, H., Zhang, Q., Zhang, Q., Chen, C., Wang, L., Wei, Z., Zhou, S., Parworth, C., Zheng, B., Canonaco, F., Prévôt, A. S. H., Chen, P., Zhang, H., Wallington, T. J. and He, K.: Wintertime aerosol chemistry and haze evolution in an extremely polluted city of the North China Plain: Significant contribution from coal and biomass combustion, Atmos. Chem. Phys., 17(7), 4751–4768, doi:10.5194/acp-17-4751-2017, 2017a.
Li, J., Zhang, M., Wu, F., Sun, Y. and Tang, G.: Assessment of the impacts of aromatic VOC emissions and yields of SOA on SOA concentrations with the air quality model RAMS-CMAQ, Atmos. Environ., 158, 105–115, doi:10.1016/j.atmosenv.2017.03.035, 2017b.
Li, J., Qi, Z., Li, M., Wu, D., Zhou, C., Lu, S., Yan, J. and Li, X.: Physical and Chemical Characteristics of Condensable Particulate Matter from an Ultralow-Emission Coal-Fired Power Plant, Energy and Fuels, 31(2), 1778–1785, doi:10.1021/acs.energyfuels.6b02919, 2017c.
Li, J., Li, X., Zhou, C., Li, M., Lu, S., Yan, J. and Qi, Z.: Study on the Influencing Factors of the Distribution Characteristics of Polycyclic Aromatic Hydrocarbons in Condensable Particulate Matter, Energy and Fuels, 31(12), 13233–13238, doi:10.1021/acs.energyfuels.7b01991, 2017d.
Li, J.: Experimental study on emission characteristics of condensable particulate matter and typical organic pollutants in coal-fired flue gas., Ph.D. thesis, School of Energy Engineering, Zhejiang University, China, 164 pp., 2018.
Li, X., Qiao, Y., Zhu, J., Shi, L. and Wang, Y.: The “APEC blue” endeavor: Causal effects of air pollution regulation on air quality in China, J. Clean. Prod., 168, 1381–1388, doi:10.1016/j.jclepro.2017.08.164, 2017e.
Li, Y., Ye, C., Liu, J., Zhu, Y., Wang, J., Tan, Z., Lin, W., Zeng, L. and Zhu, T.: Observation of regional air pollutant transport between the megacity Beijing and the North China Plain, Atmos. Chem. Phys., 16(22), 14265–14283, doi:10.5194/acp-16-14265-2016, 2016.
Li, X., Zhou, C., Li, J., Lu, S. and Yan, J.: Distribution and emission characteristics of filterable and condensable particulate matter before and after a low-low temperature electrostatic precipitator, Environ. Sci. Pollut. Res., 26(13),

12798–12806, doi:10.1007/s11356-019-04570-y, 2019.
Li, Y., Tan, Z., Ye, C., Wang, J., Wang, Y., Zhu, Y., Liang, P., Chen, X., Fang, Y., Han, Y., Wang, Q., He, D., Wang, Y. and Zhu, T.: Using wavelet transform to analyse on-road mobile measurements of air pollutants: A case study to evaluate vehicle emission control policies during the 2014 APEC summit, Atmos. Chem. Phys., 19(22), 13841–13857, doi:10.5194/acp-19-13841-2019, 2019.
Liang, P., Zhu, T., Fang, Y., Li, Y., Han, Y., Wu, Y., Hu, M. and Wang, J.: The role of meteorological conditions and pollution control strategies in reducing air pollution in Beijing during APEC 2014 and Victory Parade 2015, Atmos. Chem. Phys., 17(22), 13921–13940, doi:10.5194/acp-17-13921-2017, 2017.
Lin, C. Q., Liu, G., Lau, A. K. H., Li, Y., Li, C. C., Fung, J. C. H. and Lao, X. Q.: High-resolution satellite remote sensing of provincial $PM_{2.5}$ trends in China from 2001 to 2015, Atmos. Environ., 180, 110–116, doi:10.1016/j.atmosenv.2018.02.045, 2018.
Liu, Z., Gao, W., Yu, Y., Hu, B., Xin, J., Sun, Y., Wang, L., Wang, G., Bi, X., Zhang, G., Xu, H., Cong, Z., He, J., Xu, J., and Wang, Y.: Characteristics of $PM_{2.5}$ mass concentrations and chemical species in urban and background areas of china: Emerging results from the CARE-china network, Atmos. Chem. Phys., 18(12), 8849-8871, doi:10.5194/acp-18-8849-2018, 2018.
Lu, Q., Zhao, Y., and Robinson, A. L.: Comprehensive organic emission profiles for gasoline, diesel, and gas-turbine engines including intermediate and semi-volatile organic compound emissions, Atmos. Chem. Phys., 18(23), 17637-17654, doi:http://dx.doi.org/10.5194/acp-18-17637-2018, 2018.
Lu, C. M., Dat, N. D., Lien, C. K., Chi, K. H. and Chang, M. B.: Characteristics of Fine Particulate Matter and Polycyclic Aromatic Hydrocarbons Emitted from Coal Combustion Processes, Energy and Fuels, 33(10), 10247–10254, doi:10.1021/acs.energyfuels.9b02201, 2019.
Lu, Q., N. Murphy, B., Qin, M., J. Adams, P., Zhao, Y., O. T. Pye, H., Efstathiou, C., Allen, C. and L. Robinson, A.: Simulation of organic aerosol formation during the CalNex study: Updated mobile emissions and secondary organic aerosol parameterization for intermediate-volatility organic compounds, Atmos. Chem. Phys., 20(7), 4313–4332, doi:10.5194/acp-20-4313-2020, 2020.
Morino, Y., Chatani, S., Tanabe, K., Fujitani, Y., Morikawa, T., Takahashi, K., Sato, K. and Sugata, S.: Contributions of Condensable Particulate Matter to Atmospheric Organic Aerosol over Japan, Environ. Sci. Technol., 52(15), 8456–8466, doi:10.1021/acs.est.8b01285, 2018.
Murphy, B. N. and Pandis, S. N.: Simulating the formation of semivolatile primary and secondary organic aerosol in a regional chemical transport model, Environ. Sci. Technol., 43(13), 4722–4728, doi:10.1021/es803168a, 2009.
Murphy, B. N., Woody, M. C., Jimenez, J. L., Carlton, A. M. G., Hayes, P. L., Liu, S., Ng, N. L., Russell, L. M., Setyan, A., Xu, L., Young, J., Zaveri, R. A., Zhang, Q. and Pye, H. O. T.: Semivolatile POA and parameterized total combustion SOA in CMAQv5.2: Impacts on source strength and partitioning, Atmos. Chem. Phys., 17(18), 11107–11133, doi:10.5194/ACP-17-11107-2017, 2017.
Murphy, B. N., Nolte, C. G., Sidi, F., Bash, J. O., Appel, K. W., Jang, C., Kang, D., Kelly, J., Mathur, R., Napelenok, S., Pouliot, G. and Pye, H. O. T.: The detailed emissions scaling, isolation, and diagnostic (DESID) module in the Community Multiscale Air Quality (CMAQ) modeling system version 5.3.2, Geosci. Model Dev., 14(6), 3407–3420, doi:10.5194/gmd-14-3407-2021, 2021.
Odum, J. R., Hoffmann, T., Bowman, F., Collins, D., Flagan, R. C. and Seinfeld, J. H.: Gas/Particle Partitioning and Secondary Organic Aerosol Yields, Environ. Sci. Technol., 30, 2580–2585, doi:10.1021/ES950943+, 1996.
Pankow, J. F.: An absorption model of gas/particle partitioning of organic compounds in the atmosphere, Atmos. Environ., 28(2), 185–188, doi:10.1016/1352-2310(94)90093-0, 1994.
Pei, B.: Determination and emission of condensable particulate matter from coal-fired power plants, Huanjing Kexue/Environmental Sci., 36(5), 1544–1549, doi:10.13227/j.hjkx.2015.05.005, 2015.
Pennington, E., Seltzer, K., Murphy, B., Qin, M., Seinfeld, J. and Pye, H.: Modeling secondary organic aerosol formation from volatile chemical products, Atmos. Chem. Phys., (July), 1–26, doi:10.5194/acp-2021-547, 2021.
Pope, C. A., Burnett, R. T., Thun, M. J., Calle, E. E., Krewski, D., Ito, K. and Thurston, G. D.: Lung cancer,

cardiopulmonary mortality, and long-term exposure to fine particulate air pollution, J. Am. Med. Assoc., 287(9), 1132–1141, doi:10.1001/jama.287.9.1132, 2002.

Pye, H. O. T., Pinder, R. W., Piletic, I. R., Xie, Y., Capps, S. L., Lin, Y., Surratt, J. D., Zhang, Z., Gold, A., Luecken, D. J., Hutzell, W. T., Jaoui, M., Offenberg, J. H., Kleindienst, T. E., Lewandowski, M., and Edney, E. O.: Epoxide pathways improve model predictions of isoprene markers and reveal key role of acidity in aerosol formation. Environmental Science & Technology, 47(19), 11056-11064, https://doi.org/10.1021/es402106h, 2013.

Pye, H. O. T., Murphy, B. N., Xu, L., Ng, N. L., Carlton, A. G., Guo, H., Weber, R., Vasilakos, P., Appel, K. W., Budisulistiorini, S. H., Surratt, J. D., Nenes, A., Hu, W., Jimenez, J. L., Isaacman-VanWertz, G., Misztal, P. K., and Goldstein, A. H.: On the implications of aerosol liquid water and phase separation for organic aerosol mass, Atmos. Chem. Phys., 17, 343–369, https://doi.org/10.5194/acp-17-343-2017, 2017.

Qi, Z., Li, J., Wu, D., Xie, W., Li, X. and Liu, C.: Particulate Matter Emission Characteristics and Removal Efficiencies of a Low-Low Temperature Electrostatic Precipitator, Energy and Fuels, 31(2), 1741–1746, doi:10.1021/acs.energyfuels.6b02692, 2017.

Qin, M., Murphy, B. N., Isaacs, K. K., McDonald, B. C., Lu, Q., McKeen, S. A., Koval, L., Robinson, A. L., Efstathiou, C., Allen, C. and Pye, H. O. T.: Criteria pollutant impacts of volatile chemical products informed by near-field modelling, Nat. Sustain., 4(2), 129–137, doi:10.1038/s41893-020-00614-1, 2021.

Robinson, A. L., Donahue, N. M., Shrivastava, M. K., Weitkamp, E. A., Sage, A. M., Grieshop, A. P., Lane, T. E., Pierce, J. R. and Pandis, S. N.: Rethinking organic aerosols: Semivolatile emissions and photochemical aging, Science (80-.)., 315(5816), 1259–1262, doi:10.1126/science.1133061, 2007.

Shrivastava, M., Fast, J., Easter, R., Gustafson, W. I., Zaveri, R. A., Jimenez, J. L., Saide, P. and Hodzic, A.: Modeling organic aerosols in a megacity: Comparison of simple and complex representations of the volatility basis set approach, Atmos. Chem. Phys., 11(13), 6639–6662, doi:10.5194/acp-11-6639-2011, 2011.

Shrivastava, M. K., Lane, T. E., Donahue, N. M., Pandis, S. N. and Robinson, A. L.: Effects of gas particle partitioning and aging of primary emissions on urban and regional organic aerosol concentrations, J. Geophys. Res. Atmos., 113(18), doi:10.1029/2007JD009735, 2008.

Simon, H., Bhave, P. V., Swall, J. L., Frank, N. H., and Malm, W. C.: Determining the spatial and seasonal variability in OM/OC ratios across the US using multiple regression. Atmos. Chem. Phys., 11(6), 2933–2949, https://doi.org/10.5194/acp-11-2933-2011, 2011.

Song, J., Lu, S., Wu, Y., Zhou, C., Li, X. and Li, J.: Migration and distribution characteristics of organic and inorganic fractions in condensable particulate matter emitted from an ultralow emission coal-fired power plant, Chemosphere, 243, 125346, doi:10.1016/j.chemosphere.2019.125346, 2020.

Sun, Y., Du, W., Wang, Q., Zhang, Q., Chen, C., Chen, Y., Chen, Z., Fu, P., Wang, Z., Gao, Z. and Worsnop, D. R.: Real-Time Characterization of Aerosol Particle Composition above the Urban Canopy in Beijing: Insights into the Interactions between the Atmospheric Boundary Layer and Aerosol Chemistry, Environ. Sci. Technol., 49(19), 11340–11347, doi:10.1021/acs.est.5b02373, 2015.

Tang, L., Qu, J. B., Mi, Z. F., Bo, X., Chang, X. Y., Anadon, L. D., Wang, S. Y., Xue, X. D., Li, S. B., Wang, X., and Zhao, X. H.: Substantial emission reductions from Chinese power plants after the introduction of ultra-low emissions standards, Nat. Energy, 4, 929–938, https://doi.org/10.1038/s41560-019-0468-1, 2019.

Veld, M. in t., Alastuey, A., Pandolfi, M., Amato, F., Pérez, N., Reche, C., Via, M., Minguillón, M. C., Escudero, M. and Querol, X.: Compositional changes of PM2.5 in NE Spain during 2009–2018: A trend analysis of the chemical composition and source apportionment, Sci. Total Environ., 795, doi:10.1016/j.scitotenv.2021.148728, 2021.

Wang, G., Deng, J., Ma, Z., Hao, J. and Jiang, J.: Characteristics of filterable and condensable particulate matter emitted from two waste incineration power plants in China, Sci. Total Environ., 639, 695–704, doi:10.1016/j.scitotenv.2018.05.105, 2018.

Wang, G., Deng, J., Zhang, Y., Li, Y., Ma, Z., Hao, J. and Jiang, J.: Evaluating Airborne Condensable Particulate Matter Measurement Methods in Typical Stationary Sources in China, Environ. Sci. Technol., 54(3), 1363–1371, doi:10.1021/acs.est.9b05282, 2020a.

817 Wang, K., Yang, L., Li, J., Sheng, Z., He, Q. and Wu, K.: Characteristics of condensable particulate matter before and
818 after wet flue gas desulfurization and wet electrostatic precipitator from ultra-low emission coal-fired power plants in
819 China, Fuel, 278(June), 118206, doi:10.1016/j.fuel.2020.118206, 2020b.
820 Wang, L. Q., Chen, X., Zhang, Y. B., Li, M. Y., Li, P. F., Jiang, L. H., Xia, Y., Li, Z., Li, J. L., Wang L., Hou, T. Y., Liu
821 W. P., Rosenfeld D., Zhu T., Zhang Y. H., Chen J. M., Wang S. X., Huang Y. L., Seinfeld, J. H., and Yu, S. C.:
822 Switching to electric vehicles can lead to significant reductions of $PM_{2.5}$ and NO_2 across China, One Earth, 4, 1037–
823 1048, https://doi.org/10.1016/j.oneear.2021.06.008, 2021.
824 Wang, L. Q., Li, M. Y., Yu, S. C., Chen, X., Li, Z., Zhang, Y. B., Jiang, L. H., Xia, Y., Li, J. L., Liu W. P., Li, P. F., Eric,
825 L., Rosenfeld, D., and Seinfeld, J. H.: Unexpected rises of ozone in urban and rural areas and sulfur dioxide in rural
826 areas during the coronavirus city lockdown in Hangzhou, China: Implications for air quality, Environ. Chem. Lett.,
827 18:1713–1723, doi: 10.1007/s10311-020-01028-3, 2020c.
828 Wen, W., Cheng, S., Chen, X., Wang, G., Li, S., Wang, X., and Liu, X.: Impact of emission control on PM and the
829 chemical composition change in Beijing-Tianjin-Hebei during the APEC summit 2014, Environ. Sci. Pollut. R., 23,
830 4509–4521, doi: 10.1007/s11356-015-5379-5, 2016.
831 Wu, B., Bai, X., Liu, W., Lin, S., Liu, S., Luo, L., Guo, Z., Zhao, S., Lv, Y., Zhu, C., Hao, Y., Liu, Y., Hao, J., Duan, L.
832 and Tian, H.: Non-Negligible Stack Emissions of Noncriteria Air Pollutants from Coal-Fired Power Plants in China:
833 Condensable Particulate Matter and Sulfur Trioxide, Environ. Sci. Technol., 54(11), 6540–6550,
834 doi:10.1021/acs.est.0c00297, 2020.
835 Wu, L., Wang, X., Lu, S., Shao, M. and Ling, Z.: Emission inventory of semi-volatile and intermediate-volatility organic
836 compounds and their effects on secondary organic aerosol over the Pearl River Delta region, Atmos. Chem. Phys.,
837 19(12), 8141–8161, doi:10.5194/acp-19-8141-2019, 2019.
838 Wu, Y., Wang, P., Yu, S., Wang, L., Li, P., Li, Z., Mehmood, K., Liu, W., Wu, J., Lichtfouse, E., Rosenfeld, D. and
839 Seinfeld, J. H.: Residential emissions predicted as a major source of fine particulate matter in winter over the Yangtze
840 River Delta, China, Environ. Chem. Lett., 16(3), 1117–1127, doi:10.1007/S10311-018-0735-6/TABLES/3, 2018.
841 Xu, L., Pye, H. O. T., He, J., Chen, Y., Murphy, B. N., and Ng, N. L.: Experimental and model estimates of the
842 contributions from biogenic monoterpenes and sesquiterpenes to secondary organic aerosol in the southeastern United
843 States, Atmos. Chem. Phys., 18, 12613–12637, https://doi.org/10.5194/acp-18-12613-2018, 2018.
844 Xu, W. Q., Sun, Y. L., Chen, C., Du, W., Han, T. T., Wang, Q. Q., Fu, P. Q., Wang, Z. F., Zhao, X. J., Zhou, L. B., Ji, D.
845 S., Wang, P. C. and Worsnop, D. R.: Aerosol composition, oxidation properties, and sources in Beijing: Results from
846 the 2014 Asia-Pacific Economic Cooperation summit study, Atmos. Chem. Phys., 15(23), 13681–13698,
847 doi:10.5194/acp-15-13681-2015, 2015.
848 Yang, F., Li, Z., Liu, H., Feng, P., Tan, H., Zhang, S. and Lu, X.: Emission characteristics of condensable particulate
849 matter and sulfur trioxide from coal-fired power plants, J. Energy Inst., 94, 146–156, doi:10.1016/j.joei.2020.12.003,
850 2021.
851 Yang, H. H., Kuei-Ting Lee, Hsieh, Y.-S., Luo, S.-W. and Li, M.-S.: Filterable and Condensable Fine Particulate
852 Emissions from Stationary Sources, Aerosol Air Qual. Res., 14, 2010–2016, doi:10.4209/aaqr.2014.08.0175, 2014.
853 Yang, H. H., Arafath, S. M., Lee, K. T., Hsieh, Y. S. and Han, Y. Te: Chemical characteristics of filterable and
854 condensable $PM_{2.5}$ emissions from industrial boilers with five different fuels, Fuel, 232(168), 415–422,
855 doi:10.1016/j.fuel.2018.05.080, 2018a.
856 Yang, H. H., Arafath, S. M., Wang, Y. F., Wu, J. Y., Lee, K. T. and Hsieh, Y. S.: Comparison of Coal- and Oil-Fired
857 Boilers through the Investigation of Filterable and Condensable PM2.5 Sample Analysis, Energy and Fuels, 32(3),
858 2993–3002, doi:10.1021/acs.energyfuels.7b03541, 2018b.
859 Yu, S., Mathur, R., Pleim, J., Wong, D., Gilliam, R., Alapaty, K., Zhao, C. and Liu, X.: Aerosol indirect effect on the grid-
860 scale clouds in the two-way coupled WRF-CMAQ: Model description, development, evaluation and regional analysis,
861 Atmos. Chem. Phys., 14(20), 11247–11285, doi:10.5194/acp-14-11247-2014, 2014.
862 Zhang, Y., Tang, L., Croteau, P. L., Favez, O., Sun, Y., Canagaratna, M. R., Wang, Z., Couvidat, F., Albinet, A., Zhang,
863 H., Sciare, J., Prévôt, A. S. H., Jayne, J. T. and Worsnop, D. R.: Field characterization of the PM2.5 Aerosol Chemical

Speciation Monitor: Insights into the composition, sources, and processes of fine particles in eastern China, Atmos. Chem. Phys., 17(23), 14501–14517, doi:10.5194/acp-17-14501-2017, 2017.

Zhang, Y., Chen, X., Yu, S., Wang, L., Li, Z., Li, M., Liu, W., Li, P., Rosenfeld, D. and Seinfeld, J. H.: City-level air quality improvement in the Beijing-Tianjin-Hebei region from 2016/17 to 2017/18 heating seasons: Attributions and process analysis, Environ. Pollut., 274, 116523, doi:10.1016/j.envpol.2021.116523, 2021.

Zhao, B., Wang, S., Donahue, N. M., Jathar, S. H., Huang, X., Wu, W., Hao, J., and Robinson, A. L.: Quantifying the effect of organic aerosol aging and intermediate-volatility emissions on regional-scale aerosol pollution in China, Sci. Rep., 6, 28815, https://doi.org/10.1038/srep28815, 2016.

Zhao, B., Wu, W., Wang, S., Xing, J., Chang, X., Liou, K. N., Jiang, J. H., Gu, Y., Jang, C., Fu, J. S., Zhu, Y., Wang, J., Lin, Y. and Hao, J.: A modeling study of the nonlinear response of fine particles to air pollutant emissions in the Beijing-Tianjin-Hebei region, Atmos. Chem. Phys., 17(19), 12031–12050, doi:10.5194/acp-17-12031-2017, 2017.

Zhao, Y., Nguyen, N. T., Presto, A. A., Hennigan, C. J., May, A. A. and Robinson, A. L.: Intermediate Volatility Organic Compound Emissions from On-Road Diesel Vehicles: Chemical Composition, Emission Factors, and Estimated Secondary Organic Aerosol Production, Environ. Sci. Technol., 49(19), 11516–11526, doi:10.1021/acs.est.5b02841, 2015.

Zheng, C., Hong, Y., Liu, S., Yang, Z., Chang, Q., Zhang, Y., and Gao, X.: Removal and emission characteristics of condensable particulate matter in an ultralow emission power plant, Energy & Fuels, 32(10), 10586-10594, https://doi.org/10.1021/acs.energyfuels.8b02464, 2018.

Zheng, H., Cai, S., Wang, S., Zhao, B., Chang, X. and Hao, J.: Development of a unit-based industrial emission inventory in the Beijing-Tianjin-Hebei region and resulting improvement in air quality modeling, Atmos. Chem. Phys., 19(6), 3447–3462, doi:10.5194/acp-19-3447-2019, 2019.

Zhou, C.: Experimental study on emission and distribution characteristics of organic pollutants in condensable particulate matter in coal-fired flue gas., Master thesis, School of Energy Engineering, Zhejiang University, China, 82 pp., 2019.

Table 1 Definitions of some acronyms used in this study.

Acronyms	Definitions
FPM	Primary-emitted filterable particulate matter which is in liquid or solid phases in flue
CPM	Primary-emitted condensable particulate matter which is in gas phase at flue gas temperature but condenses or reacts in the ambient air to form solid or liquid PM
OM (CPM)	Organic matter measured in CPM
OM_{si} (CPM)	Organic matter in CPM which is semi-volatile (SVOCs, $10^0 \leq C^* \leq 10^3$ μg m^{-3}), or has intermediate volatility (IVOCs, $10^3 < C^* \leq 10^6$ μg m^{-3}) are combined as OM_{si} (CPM)
OM ($C^* \leq 100$)	Organic matter with the saturation concentrations (C^*) below 100 μg m^{-3}
SVOCs	Primary-emitted semi-volatile organic compounds
IVOCs	Primary-emitted intermediate-volatility organic compounds
S/IVOCs	SVOCs + IVOCs
POA	Atmospheric organic aerosol from primary-emitted organic matter or formed by condensation of organic vapors before photochemical reactions
SOA	Atmospheric secondary organic aerosol generated by photochemical reactions and condensation of organic vapors after photochemical reactions
ASOA	SOA generated by photochemical oxidations of anthropogenic volatile organic compounds
BSOA	SOA generated by photochemical oxidations of biogenic volatile organic compounds
SISOA	SOA generated by photochemical oxidations of primary S/IVOCs
OA	POA + SOA

Table 2 List of the ratios of the emission rates of OM in condensable particulate matter (CPM) (E_{OM}(CPM)) to those of $PM_{2.5}$ in filterable particulate matter (FPM) ($E_{PM2.5}$(FPM)) from stationary combustion sources based on the collected references.

method	emission sources	number	E_{OM}(CPM)/ $E_{PM2.5}$(FPM)			references
			[Min, Max]	Mean ± SD	median	
cooling method (EPA 202)	coal-fired power plant	30	[0.01, 25.4]	6.87 ± 7.25	3.99	Li et al. (2017c, 2017d); Li (2018); Li et al. (2019); Lu et al. (2019); Pei (2015); Qi et al. (2017); Song et al. (2020); Wang et al. (2020b); Wu et al. (2020); Yang et al. (2014, 2018b); Yang et al.(2021); Zhou (2019)
	waste incineration power plant	2	[1.64, 4.95]	3.29 ± 1.65	3.29	Wang et al. (2018)
	industrial coal-fired boiler	6	[0.14, 1.03]	0.58 ± 0.34	0.50	Lu et al. (2019) Yang et al. (2014, 2018a, 2018b)
	heavy oil-fired boiler	4	[0.28, 2.49]	1.62 ± 0.88	1.85	Yang et al. (2018a, 2018b)
	wood-fired boiler	1		0.03		
	natural gas-fired boiler	1		6.67		Yang et al. (2018a)
	diesel-fired boiler	1		15.84		
	iron and steel plants	5	[0.32, 7.22]	3.35 ± 2.21	3.00	Yang et al. (2014, 2015)
	incinerator	1		0.12		Yang et al. (2014)
dilution method (ISO 25597)	iron and steel coking plant	1		0.416		Zhang et al. (2020)

Table 3 Probabilistic distributions with uncertainty ranges in the ratio of E_{OM}(CPM) to $E_{PM2.5}$(FPM) (95% confidence interval). Para1 represents the mean for normal, and the mean of ln(x) for lognormal. Para2 represents the standard deviation for normal, and the standard deviation of ln(x) for lognormal. Mean represents the mean for emission ratios of each source category derived from the statistical bootstrap simulation.

Input parameters	Emission sources	Distribution type	Para1	Para2	Mean	Uncertainty ranges (95% confidence level)
E_{OM}(CPM) /$E_{PM2.5}$(FPM)	Power plant	lognormal	1.07	0.93	4.12	(3.10, 5.29)
	Industry combustion	lognormal	-0.47	1.43	1.38	(0.62, 2.44)
	Steel	normal	2.80	1.98	2.80	(0.92, 4.50)
Total						(-27%, 28%)

Table 4 Simulation case design. PP, IN, IR, and TR denote source sectors of power plant, industry combustion, steel, and transportation, respectively. Three kinds of scaling factors for the five volatility bins of organic CPM are tested: fac1 (0, 0.18, 0.14, 0.18, 0.5), fac2 (0, 0.66, 0.40, 0.51, 1.43), and fac3 (0, 0.42, 0.27, 0.345, 0.965) which is the average of fac1 and fac2.

Simulation Cases	Aerosol module	E_{PP_OM}(CPM) /$E_{PM2.5}$(FPM)	E_{IN_OM}(CPM) /$E_{PM2.5}$(FPM)	E_{IR_OM}(CPM) /$E_{PM2.5}$(FPM)	Volatility bins
Only FPM	AERO6VBS	0	0	0	
	AERO7	0	0	0	
S1.1	AERO7	4.12	1.38	2.80	fac1
S1.2	AERO7	4.12	1.38	2.80	fac2
S1.3	AERO7	4.12	1.38	2.80	fac3
S2.1	AERO7	3.01	1.01	2.04	fac1
S2.2	AERO7	3.01	1.01	2.04	fac2
S3.1	AERO7	5.27	1.77	3.58	fac1
S3.2	AERO7	5.27	1.77	3.58	fac2
S4.2	AERO7	3.71	1.24	2.52	fac2
S5.2	AERO7	4.49	1.50	3.05	fac2
S6_TR	AERO7	0	0	0	fac1
S7_IN	AERO7	0	1.38	0	fac1
S8_IR	AERO7	0	0	2.80	fac1
S9_PP	AERO7	4.12	0	0	fac1

Table 5 Model evaluation statistics for hourly OA, POA and SOA concentrations during October 14–November 14, 2014, and daily OA concentrations during December 6–30, 2018, under different sensitivity simulation cases.

Period	City	Species	Cases	N	OBS	SIM	MB	NMB	NME	R
October 14–November 14, 2014	Beijing	OA	base	723	33.71	11.90	-21.81	-64.70%	64.84%	0.71
			S1.1		33.71	25.08	-8.63	-25.60%	47.00%	0.70
			S1.2		33.71	39.38	5.67	16.82%	58.62%	0.69
			S1.3		33.71	31.88	-1.83	-5.43%	49.63%	0.70
		POA	base	723	16.25	4.28	-11.97	-73.66%	73.75%	0.54
			S1.1		16.25	10.24	-6.01	-36.98%	54.01%	0.54
			S1.2		16.25	23.32	7.07	43.51%	87.16%	0.53
			S1.3		16.25	16.45	0.20	1.23%	61.57%	0.53
		SOA	base	723	17.46	7.62	-9.84	-56.36%	57.22%	0.74
			S1.1		17.46	14.85	-2.61	-14.95%	47.42%	0.73
			S1.2		17.46	16.05	-1.41	-8.08%	48.24%	0.73
			S1.3		17.46	15.42	-2.04	-11.68%	47.75%	0.73
December 6–30, 2018	Handan	OA	base	25	45.24	17.70	-27.54	-60.88%	60.89%	0.62
			S1.1		45.24	35.04	-10.20	-22.55%	38.00%	0.61
			S1.3		45.24	48.86	3.62	8.00%	38.95%	0.59
	Shijiazhuang	OA	base	25	42.22	18.38	-23.84	-56.47%	57.45%	0.61
			S1.1		42.22	38.88	-3.34	-7.91%	35.69%	0.61
			S1.3		42.22	58.02	15.80	37.42%	47.27%	0.61
	Xingtai	OA	base	25	42.22	13.35	-28.87	-68.38%	68.37%	0.58
			S1.1		42.22	29.34	-12.88	-30.51%	40.59%	0.58
			S1.3		42.22	42.56	0.34	0.81%	34.52%	0.56
	Dezhou	OA	base	23	41.66	15.48	-26.18	-62.84%	63.49%	0.47
			S1.1		41.66	31.25	-10.41	-24.99%	42.76%	0.54
			S1.3		41.66	42.58	0.92	2.21%	43.06%	0.56

Note: OBS and SIM denote mean concentrations (μg m^{-3}) of observations and simulations, respectively; MB: mean bias; NMB: normalized mean bias; NME: normalized mean error; R: correlation coefficient.

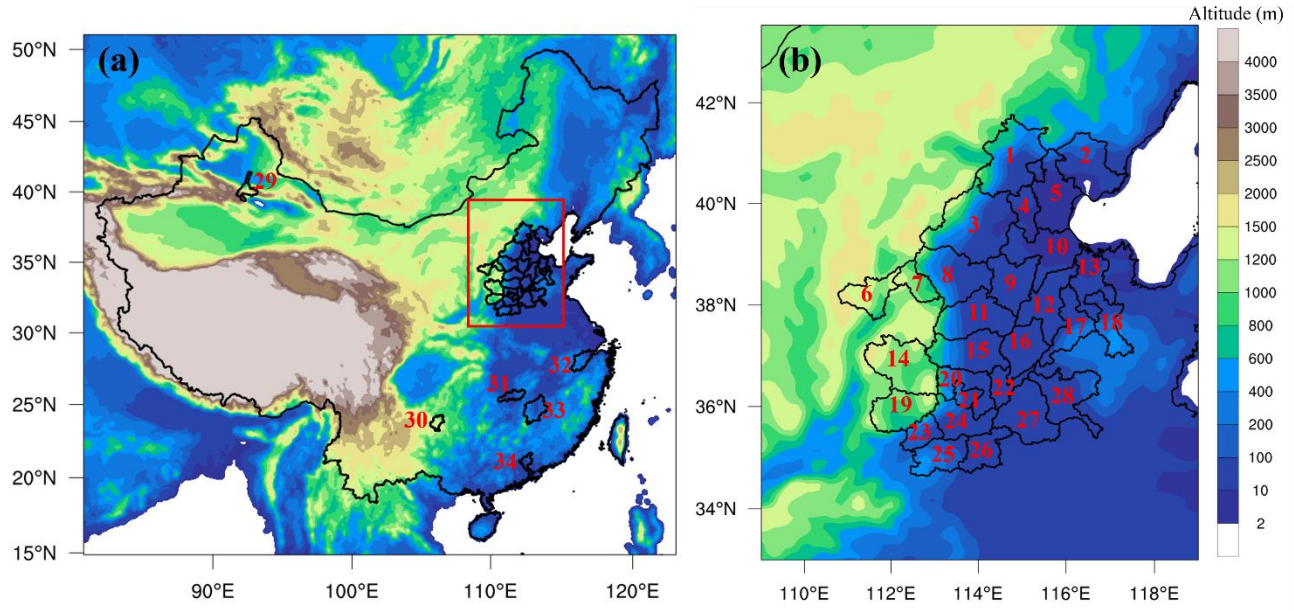

Figure 1. (a) Map of the modeling domain and location of each target city in model evaluation. (b) The locations of BTH2+26 cities, denoted as the red frame in (a). The color shading represents the regional altitude.

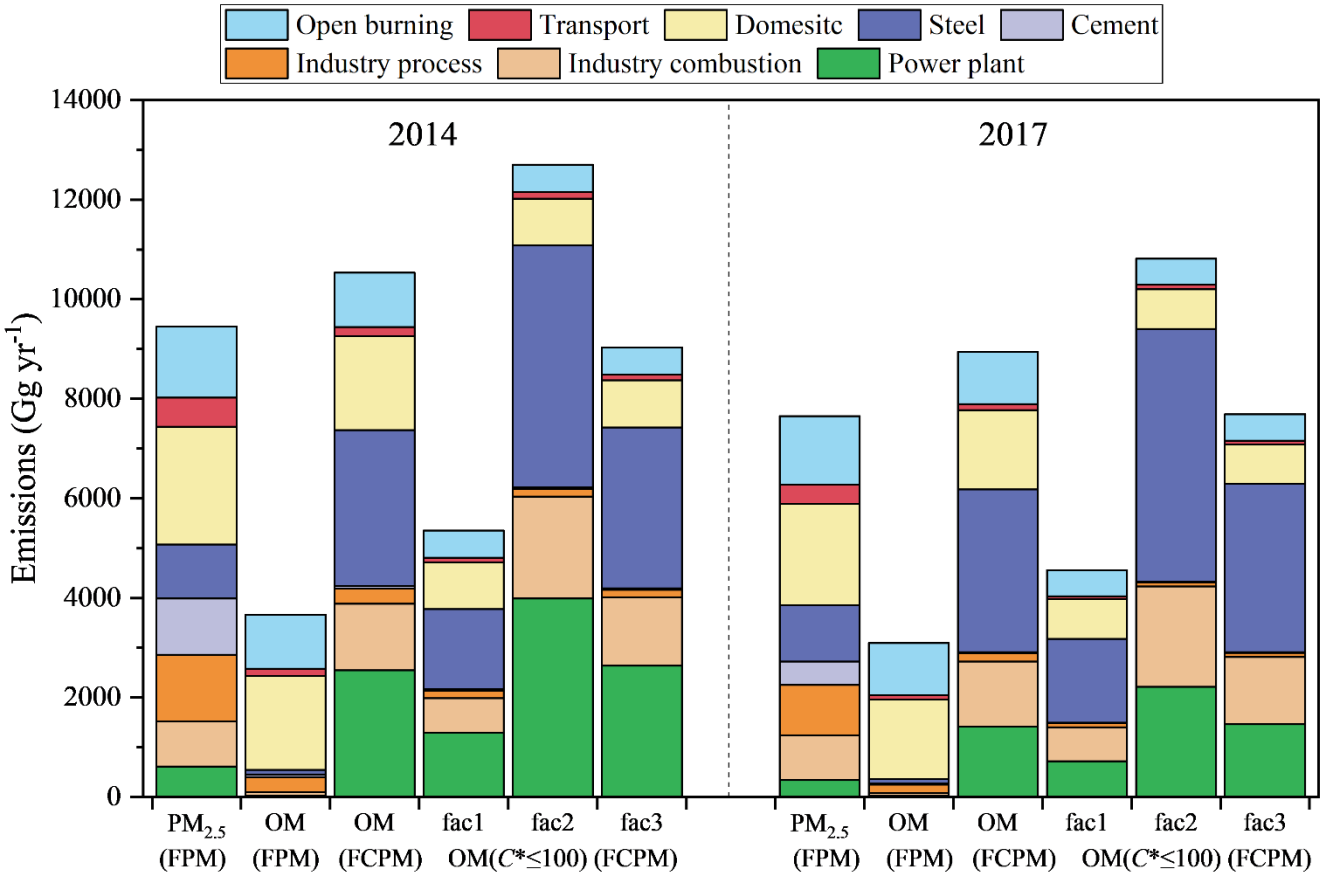

Figure 2. Annual emissions of $PM_{2.5}$ and OM in filterable particulate matter (FPM), OM in filterable plus condensable particulate matter (FCPM) before the volatility distributions, and OM (C^*≤100 μg m^{-3}) in FCPM after application of the volatility distributions for the fac1, fac2 and fac3 cases over China in 2014 and 2017.

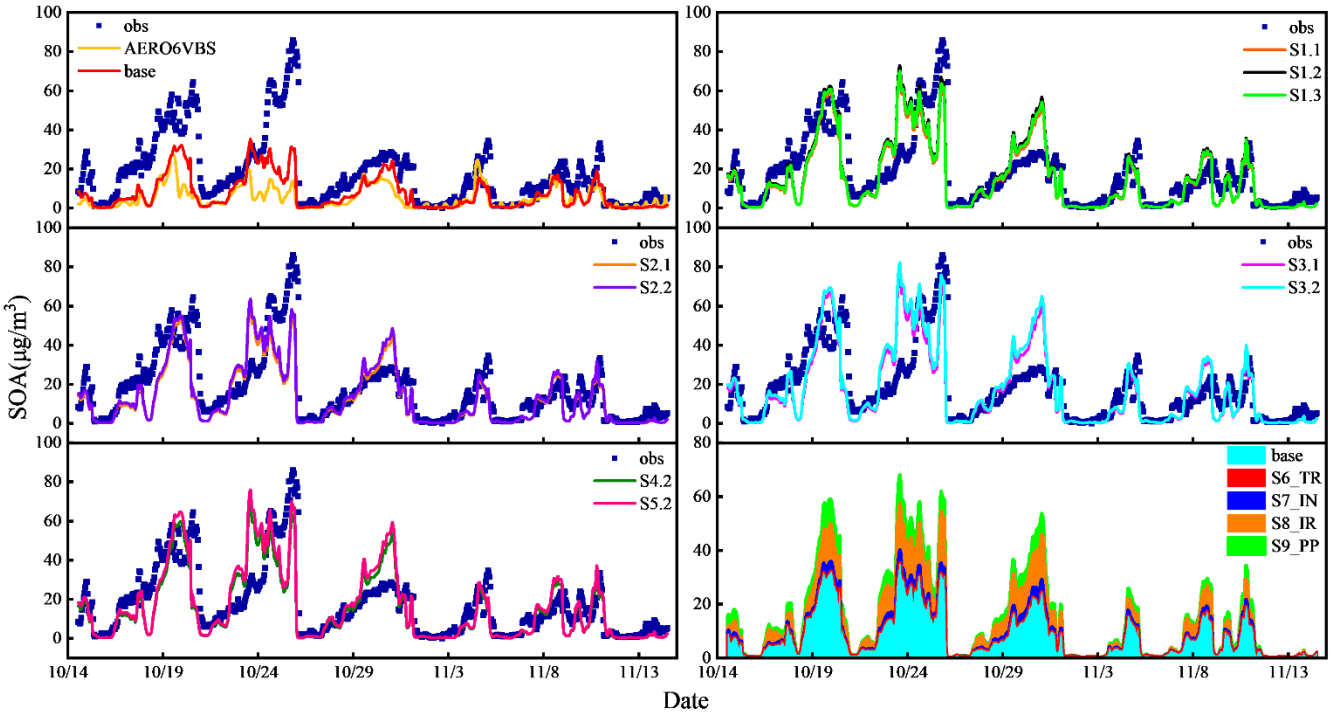

Figure 3. The observed and simulated hourly SOA concentrations during the episode from October 14 to November 14, 2014 at the Beijing site in the sensitivity cases as summarized in Table 3.

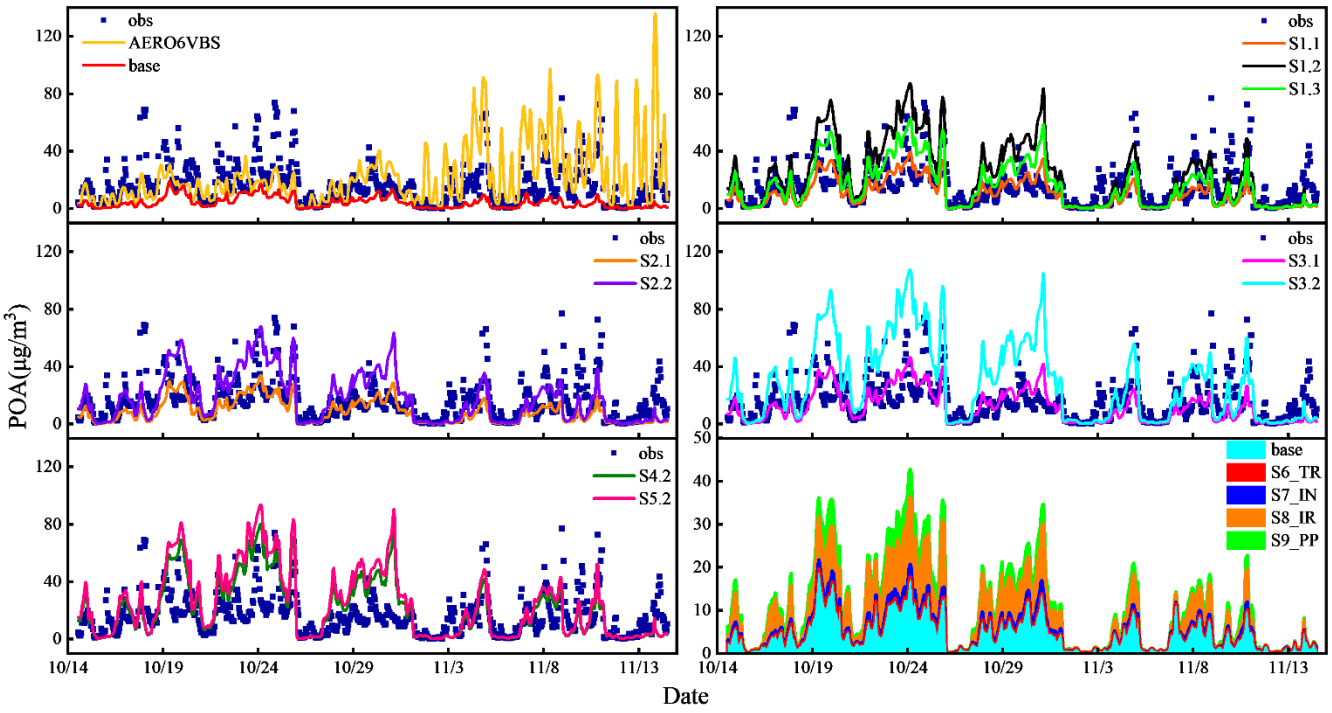

Figure 4. The observed and simulated hourly POA concentrations during the episode from October 14 to November 14, 2014 at the Beijing site in the sensitivity cases as summarized in Table 3.

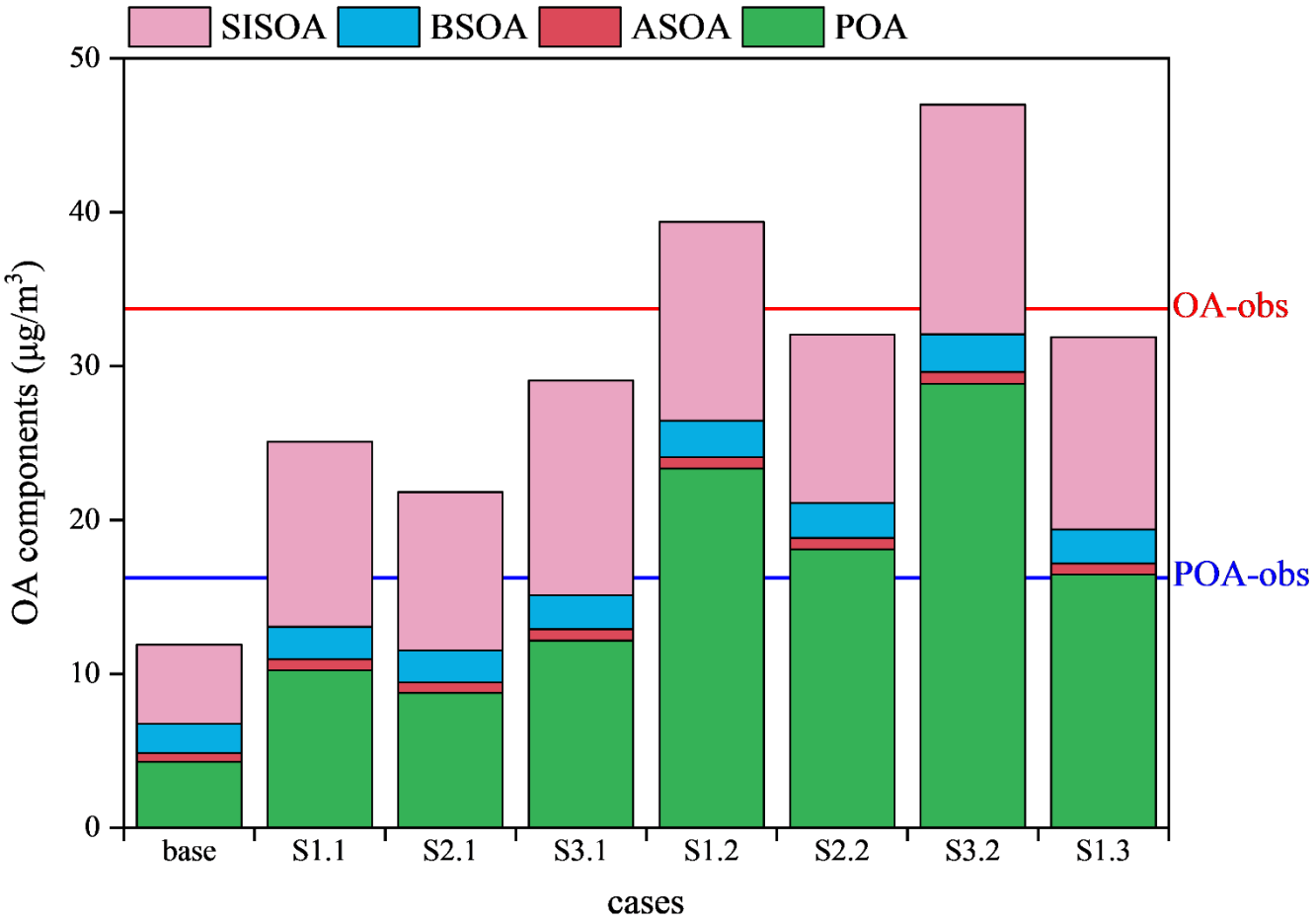

Figure 5. The simulation concentrations of different OA components averaged over the whole study period from October 14 to November 14, 2014 at the Beijing site in the sensitivity cases. AERO7_def is abbreviated as def and AERO7_adj as adj. ASOA, BSOA and SISOA denote SOA generated by anthropogenic VOCs, biogenic VOCs and low volatile S/IVOCs, respectively. The red and blue horizontal line denote the average observation concentrations of OA and POA, respectively.

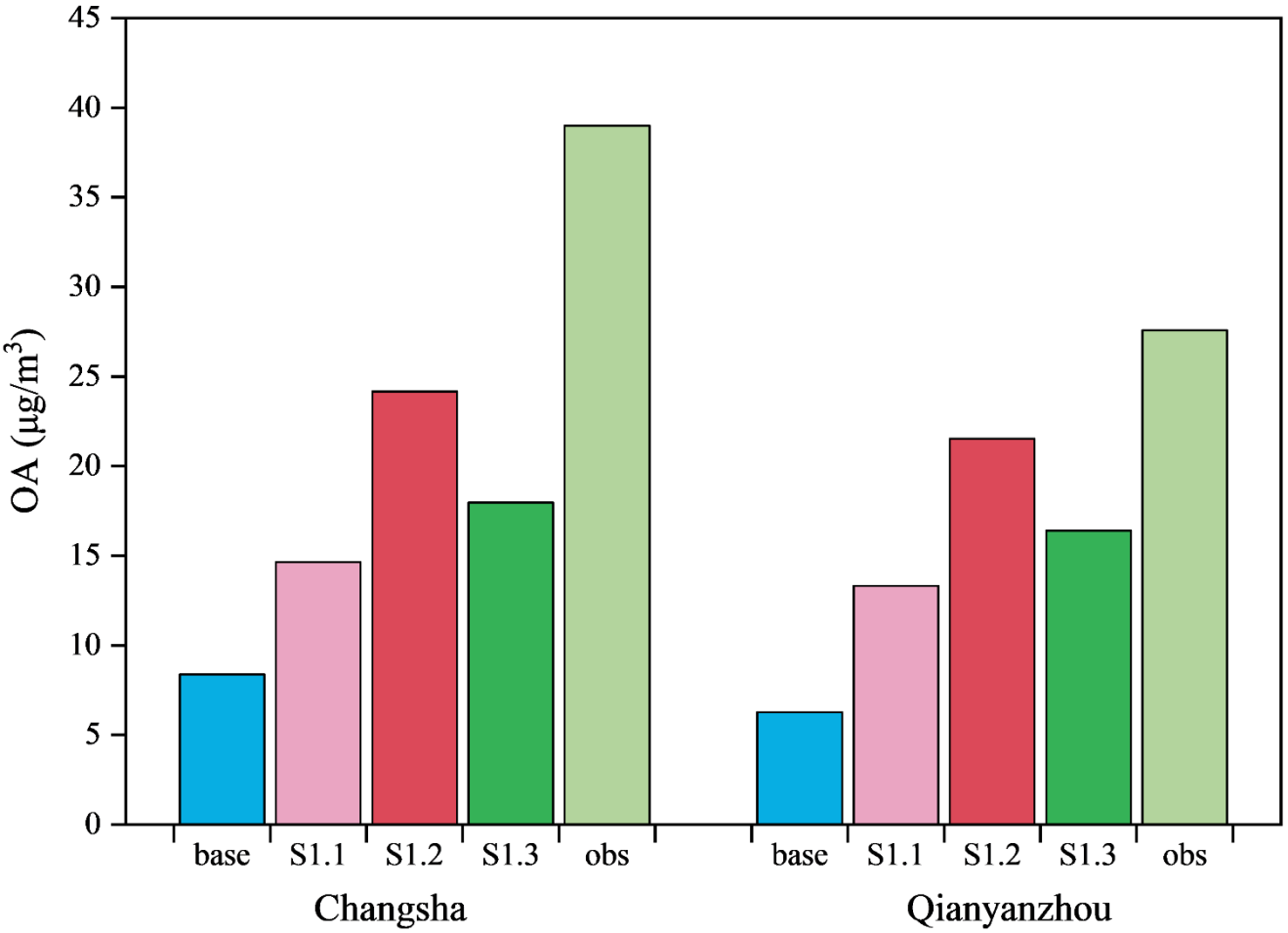

Figure 6. The observed and simulated OA concentrations in the sensitivity cases on November 3, 2014 at Changsha and Qianyanzhou.

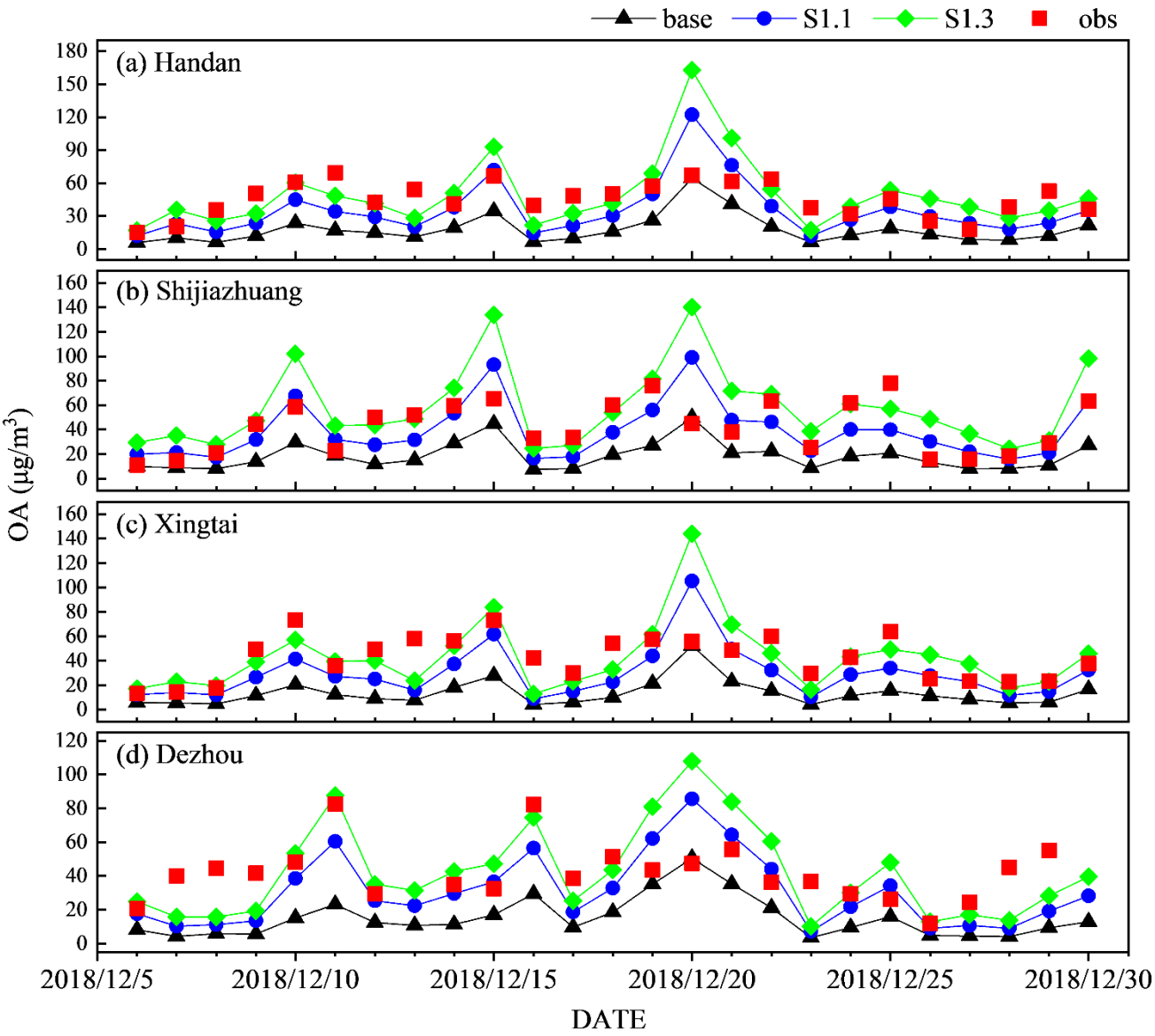

Figure 7. The observed and simulated daily OA concentrations during December 6-30 in 2018 at (a) Handan, (b) Shijiazhuang, (c) Xingtai and (d) Dezhou.

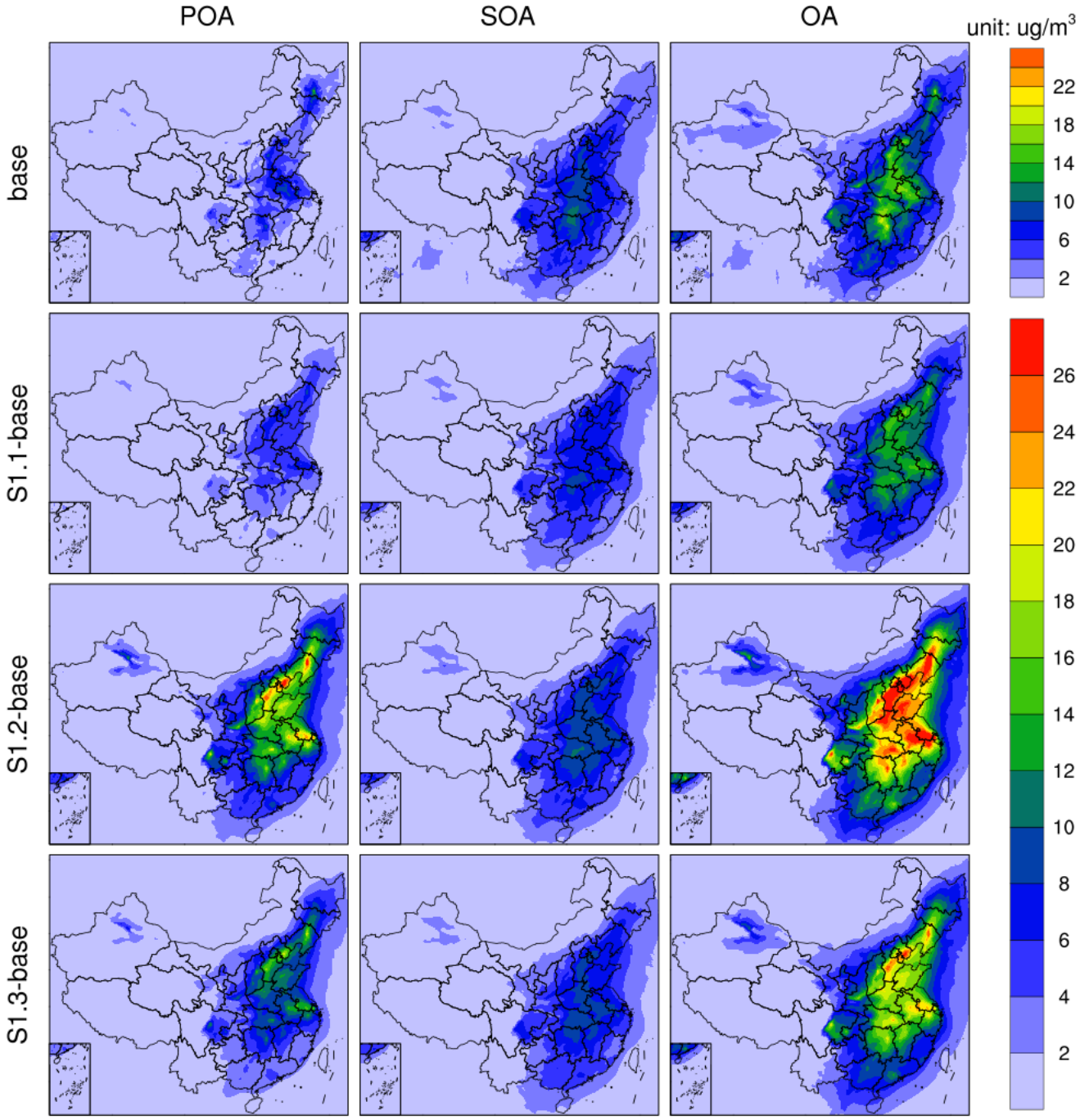

Figure 8. Spatial distributions of the concentrations of POA, SOA and OA averaged over the whole period of October 14-November 14 in 2014 generated by the simulations with FPM sources (base) and CPM sources (S1.1-base, S1.2-base, S1.3-base).

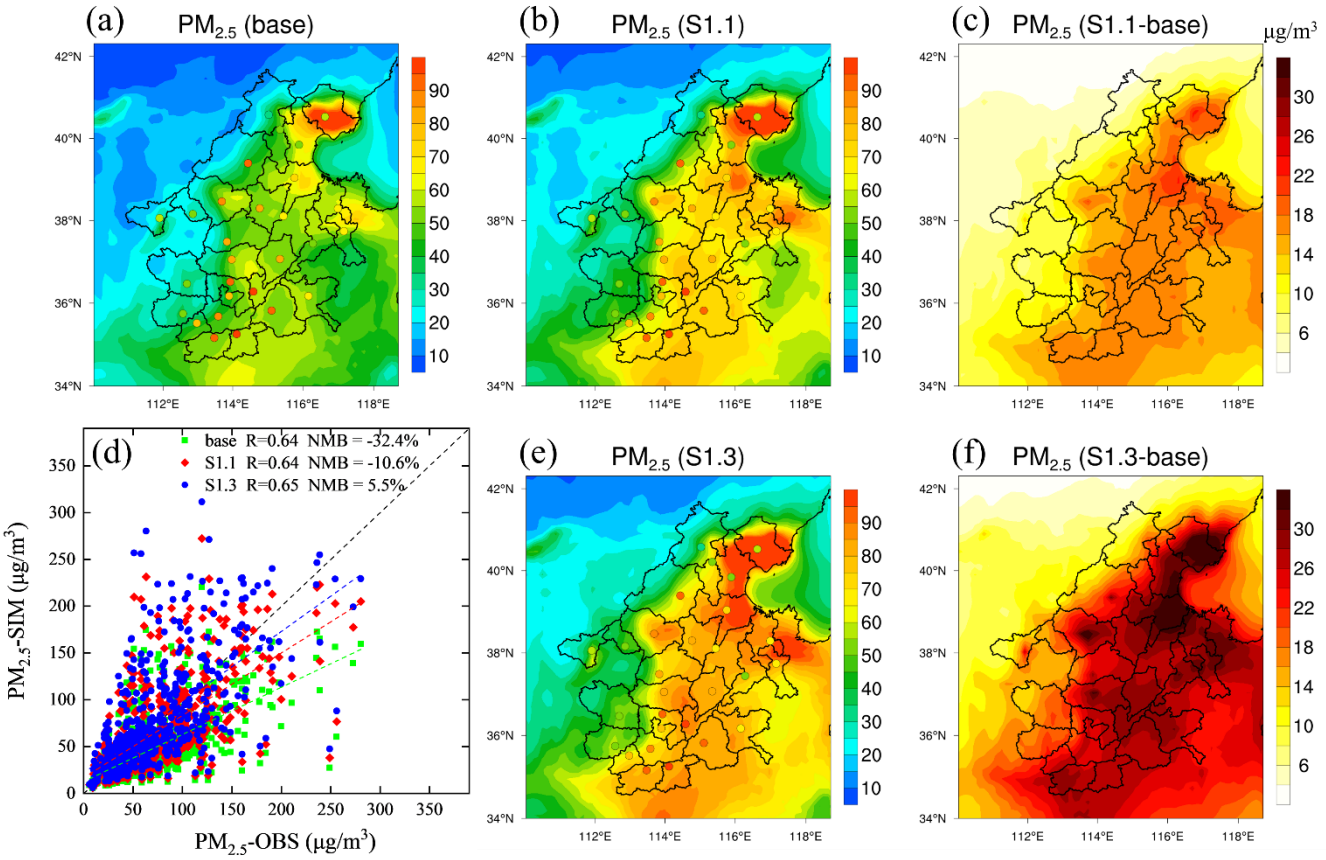

Figure 9. Spatial distributions of the average $PM_{2.5}$ concentrations during December 6-30, 2018, over the BTH2+26 cities in (a) base, (b) S1.1, (e) S1.3, (c) absolute difference between S1.1 and base, and (f) absolute difference between S1.3 and base. Among them, the $PM_{2.5}$ concentrations from December 22 to 26 are not included due to the missing observation data. (d) Scatter plots and linear regressions of observed (OBS) and simulated (SIM) daily $PM_{2.5}$ concentrations for all of the BTH2+26 cities during the above time period under the base, S1.1, and S1.3 scenarios.

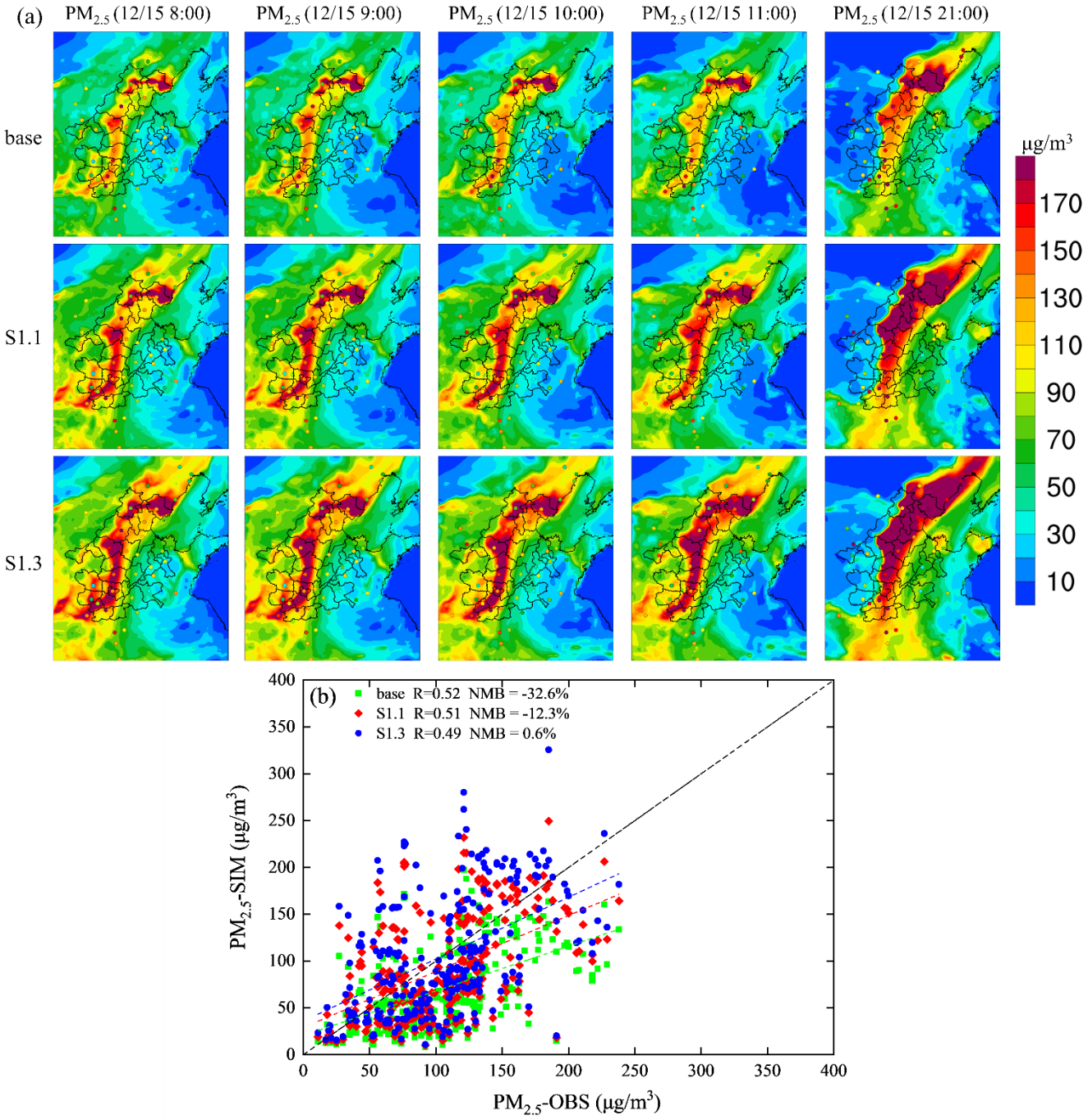

Figure 10. (a) Spatial distributions of hourly $PM_{2.5}$ concentrations at some peak hours over the BTH2+26 cities under the base, S1.1, and S1.3 scenarios. The colored dots denote observation values for each city. (b) Scatter plots and linear regressions of observed (OBS) and simulated (SIM) hourly $PM_{2.5}$ concentrations for all cities under the base, S1.1, and S1.3 scenarios.